MATERIALS CHEMISTRY FRONTIERS

CHINESE CHEMICAL SOCIETY

ROYAL SOCIETY OF CHEMISTRY

REVIEW

View Article Online
View Journal | View Issue

Check for updates

Cite this: *Mater. Chem. Front.*, 2024, **8**, 2029

Surface engineering in $CsPbX_3$ quantum dots: from materials to solar cells

Yinyan Xu,[ab] Mei Lyu[a] and Jun Zhu *[a]

Received 16th August 2023,
Accepted 25th September 2023

DOI: 10.1039/d3qm00911d

rsc.li/frontiers-materials

Lead halide perovskite quantum dots (PQDs) are considered to be one of the most promising classes of photoactive materials for solar cells due to their prominent optoelectronic properties and simple preparation techniques. Even though the high resistivity of these PQDs toward defect formation results in compelling optical properties and their manifestation in device applications, they are not free from defects, and their photoluminescence quantum yield is often not unity. Defects and ligands at the surface of PQDs play a critical role in charge transport and non-radiative recombination, which lowers the solar cell efficiency and stability. Therefore, understanding the defects and developing effective passivation routes are critical for achieving advances in device performance. In this review, we focus on the surface engineering of $CsPbX_3$ PQDs, including the formation of surface vacancy defects and the surface ligand modification of PQDs, and then summarize the corresponding surface defect passivation strategy for systematically improving the performance of PQD solar cells. At the end, a brief summary and perspective are presented looking forward to the future development of PQD solar cells.

Published on 27 de setembre 2023. Downloaded on 11/2/2026 22:48:11.

1. Introduction

Colloidal quantum dots (QDs) are chemically synthesized semiconductor nanocrystals whose sizes are in the quantum confinement regime, typically less than 10–20 nm.[1–3] Their optical and electrical properties can be easily tuned by modifying their shape and size due to the quantum confinement effect, which is difficult to achieve in bulk materials.[4,5] As a result, QDs are attracting attention as a highly flexible platform for realizing next-generation optoelectronic devices, including solar cells,[6,7] photodetectors,[8] lasers,[9] and light-emitting diodes (LEDs).[10,11] Colloidal QDs have been among the most accomplished building blocks of modern nanoscience since the last century.[12]

The unique advantages of QDs, such as wide tunability of band gaps and easy solution processability make them promising candidates for next-generation solar cells.[6,7] In addition, their theoretical efficiency has the potential to break the Shockley–Queisser limit of ~33% through multiple exciton generation.[13] In the past decades, most high-performance QD solar cells were reported from QD materials in two main categories: lead chalcogenides (PbX, X = S, Se)[14–16] and lead halide perovskites.[17,18] Before 2016, high-efficiency QD solar cells consisted primarily of PbX (X = S, Se), and recent sustained efforts culminated in a significant PCE of 13.8%.[16]

Recently, colloidal metal halide perovskite quantum dots (PQDs) (here PQD generally refers to perovskite nanocrystals with a size less than 20 nm) have emerged as another, perhaps most defect-tolerant material candidate for cost-effective and solution-processed solar cells,[17] LEDs,[19] and displays.[20] In particular, inorganic PQDs, the primary example of which is cesium lead halides ($CsPbX_3$, X = I, Br, Cl), exhibit a high photoluminescence quantum yield (PLQY), spectrally tunable bandgap, flexible compositional control, and crystalline strain benefits which opens a route for next-generation devices.[21] In 2016, Luther *et al.*[17] used $CsPbI_3$ PQDs for the first time to fabricate solar cells by a layer-by-layer deposition approach. The solar cell exhibited a high open circuit voltage (V_{OC}) of 1.23 V and a high-power conversion efficiency (PCE) of 10.77%. To date, the highest PCE achieved by PQD solar cells has reached 17.39% (certified 16.6%),[18] indicating great potential for solution-processed high performance PQD solar cells. Though PCEs of PQD solar cells have shown rapid, significant improvement, they are still limited compared to solar cells fabricated using bulk perovskite materials.[22]

The large surface-to-volume ratio of QDs plays a critical role in determining their properties and the solar cell performance.[23,24] Long-chain organic ligands, such as oleic acid (OA) or oleylamine (OAm), are used to cap the QD surface to disperse it uniformly in the colloidal system. However, long, insulating ligands trap charges within the PQDs and increase the interparticle distance, leading to poor electronic

[a] *Special Display and Imaging Technology Innovation Center of Anhui Province, Anhui Province Key Laboratory of Measuring Theory and Precision Instrument, Academy of Opto-Electric Technology, Hefei University of Technology, 193 Tunxi Road, Hefei, 230009, P. R. China. E-mail: jzhu@hfut.edu.cn*

[b] *Key Lab of Advance Functional Materials and Devices, School of Chemistry and Chemical Engineering, Hefei University of Technology, 193 Tunxi Road, Hefei, 230009, China*

Published on 27 de setembre 2023. Downloaded on 11/2/2026 22:48:11.

coupling.[25,26] Besides, the surface of PQDs always presents a large number of halogen vacancies which can act as non-radiative recombination centers of photoinduced carriers, significantly affecting the charge extraction of solar cells.[27–30] Therefore, studies of PQD surface chemistry will be essential in order to improve the performance of PQD solar cells. Although there have been some reviews on PQD solar cells in recent years,[31–35] the overviews focusing on the research of PQD surface chemistry to improve the photovoltaic performance of PQD solar cells are still scarce, which would provide insight into viable approaches to achieving high performance PQD solar cells. In this review, firstly, we analyze the reasons for the formation of defects on the surface of PQDs. Secondly, we summarize the corresponding surface defect passivation strategy for improving the performance of PQD solar cells. Thirdly, the advantages and disadvantages of various defect passivation strategies are analyzed in order to select a suitable passivation strategy. Finally, we emphasize the challenges and prospects of PQD solar cells in the future.

2. Crystal and electronic structure of PQDs

2.1 Crystal structure of PQDs

Perovskites, named after Russian mineralogist Lev Perovski, refer to a large class of materials whose crystal structure resembles that of calcium titanate ($CaTiO_3$).[36] The general chemical formula for pure perovskite compounds is ABX_3 and the typical perovskite crystal structure is usually a lattice skeleton joined by a $[BX_6]^{4-}$ octahedron through a common corner, wherein the A cation is in the void, as shown in Fig. 1a. Usually, A is a cation (typically $CH_3NH_3^+$ (MA^+), $HC(NH_2)_2^+$ (FA^+), Cs^+),[37–40] B is a metal divalent cation (Pb^{2+}, Sn^{2+}, *etc.*),[41,42] while X denotes halide anions (I^-, Br^-, Cl^-).[43–45] The perovskite crystal structure can accommodate a variety of cations and anions, forming a unique chemical structure with unique electronic properties and a controlled optical band gap, which make it ideal for many optoelectronic applications. The size of the A-site cation is crucial for determining the structure, optical behavior, and stability of the perovskite. The filling of the $[BX_6]^{4-}$ octahedral cavity with A-site cations needs to satisfy the Goldschmidt tolerance factor.[46]

$$t = \frac{r_A + r_B}{\sqrt{2}(r_B + r_X)} \quad (1)$$

where r_A, r_B, and r_X are the ionic radii of the A, B and X positions, respectively. When t is in the range of 0.813 to 1.107, the structure of the perovskite is in a stable state and is considered to be the most favorable crystal structure for forming a cuboid between 0.9 and 1.0.[47] The perovskite structure will be distorted as the tolerance factor decreases below 0.9 because of the $[BX_6]^{4-}$ octahedra tilting. The A-site cation is too large to form a perovskite configuration when $t > 1$, whereas when $t < 0.8$, the A-site cation is too small to form the perovskite. Perovskite structures are further constrained by the octahedral factor μ.

$$\mu = \frac{r_B}{r_X} \quad (2)$$

The μ describes the stability of the BX_6 octahedra, which depends on the radii of the B and X ions. The stability range for μ is between 0.442 and 0.895.[48] The tolerance and octahedral factors are currently used to predict the stability of novel possible perovskite combinations.

For $CsPbI_3$, the undesirable phase transition is because the size of the Cs^+ cation is too small (Cs^+, with an ionic radius of 1.81 Å, is considerably smaller than the organic ones MA^+ (2.70 Å) or FA^+ (2.79 Å)).[49] Therefore, since the octahedron is relatively prone to tilting or rotation, a phase change occurs and various phase structures are generated as shown in Fig. 1b. Single-cation $CsPbI_3$ systems form a thermodynamically stable yellow room temperature δ-phase (non-perovskite) before undergoing reversible, high-temperature phase transitions to their optically active black perovskite phases: α (cubic), β (tetragonal), and γ (orthorhombic).[50,51]

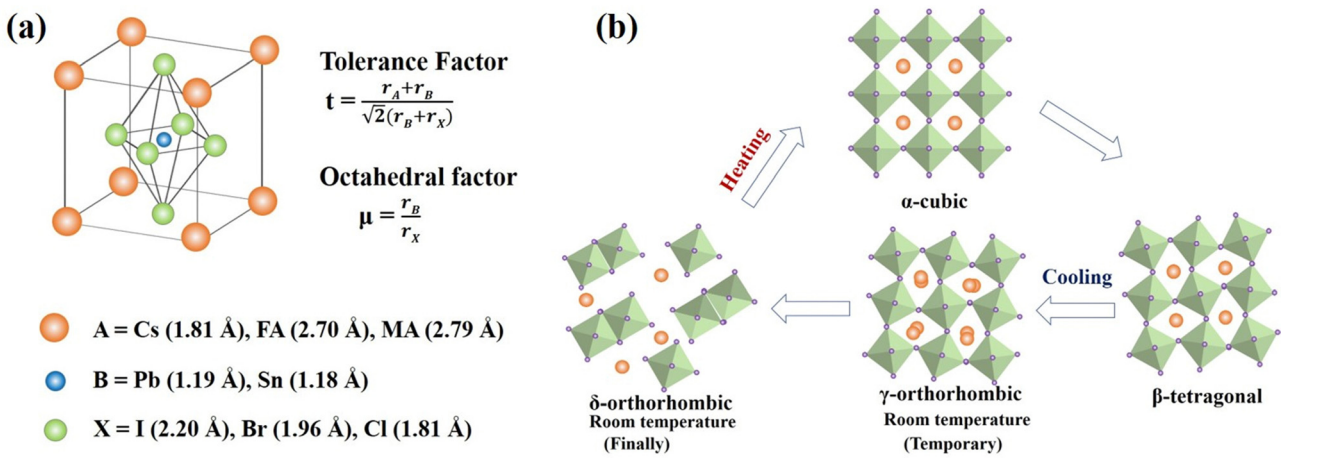

Fig. 1 (a) A cubic perovskite crystal structure (α-phase) showing flexibility in the choice of cation (A), metal (B), and anion (X), whose ionic radii are shown. (b) Schematic presentation of the structural phase transition of various polymorphs of $CsPbI_3$ as a function of temperature.

 This journal is © The Royal Society of Chemistry and the Chinese Chemical Society 2024

Published on 27 de setembre 2023. Downloaded on 11/2/2026 22:48:11.

2.2 Electronic structure of PQDs

The electronic specificity of PQDs is highly resistant to material defects and surfaces. This defect-tolerant nature is typically intrinsic, mainly attributed to the PQDs' electronic band structure, including the nature of the valence band maximum (VBM) and conduction band minimum (CBM). The VBM has antibonding properties, and the CBM is stabilized by strong spin–orbit coupling.[52,53] Fig. 2 shows a comparison between the defect tolerance mechanisms in PQD and traditional metal chalcogenide nanocrystals. The electronic structure of the $CsPbX_3$ perovskite is special. The VBM is determined by the halide 3/4/5p and Pb 6s atomic orbitals and the CBM is mainly dominated by the Pb 6p atomic orbital, resulting in a low degree of hybridization.[54] For this unique electronic structure, the interstitial and antisite defects in the PQDs hardly exist due to the high formation energy.[53,55]

2.3 Quantum confinement effect

Quantum confinement effects are also called quantum size effects. In general, when reducing the material crystallite size from bulk (with nearly infinite repetitive periodicity) to a size comparable to the radius of Bohr exciton, its electrons and holes are subjected to different confinement effects, leading to an increase in the width of the forbidden bands, which exhibits size-dependent optical and electrical properties, which is known as the quantum confinement effect.[56]

The Bohr radius of a particle is defined as $a_B = \varepsilon(m/m^*)a_0$, where ε is the dielectric constant of the material, m^* is the mass of the particle, m is the rest mass of the electron, and a_0 is the Bohr radius of the hydrogen atom.[57,58] An illustration of the quantum confinement effect has been given in Fig. 3. It shows a decreasing confinement width with decreasing size of the particle and a corresponding blue shift in emission wavelength due to the increased band gap.

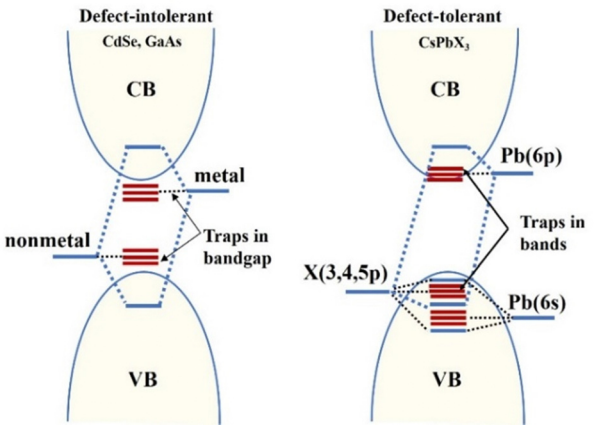

Fig. 2 Schematic representation of the electronic band structure of typical defect-intolerant semiconductors (CdSe, GaAs) and in lead halide perovskite ($CsPbX_3$).

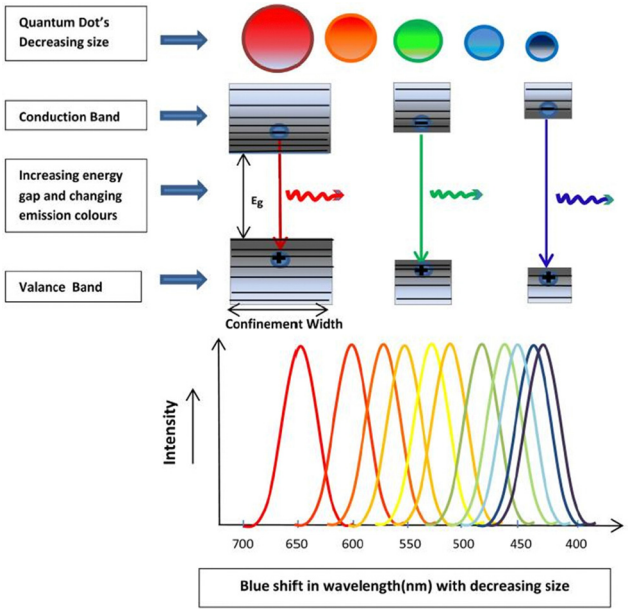

Fig. 3 Illustration of the quantum confinement effect. Reproduced with permission.[56] Copyright 1992, American Physical Society.

3. Surface engineering of PQDs

Understanding the surface chemistry of PQDs is important for gaining insight into surface passivation mechanisms that can significantly affect their optical properties and improve the performance of PQD solar cells.[59] The defect tolerance of PQDs is a major enabling factor in their bright photoluminescence. However, the PLQYs of these QDs do not yet regularly approach unity. On one hand, the termination of an extended inorganic solid crystal inherently produces under-coordinated atoms, making surface traps a ubiquitous challenge for nanocrystals.[30,60–62] Bodnarchuk *et al.*[61] firstly used density functional theory to calculate different possible surface terminations of $CsPbBr_3$ QDs and predicted the effects of different surface terminations on the electronic structures and resulting optoelectronic properties. By providing upper and lower bounds to their anion/lead (X/Pb) stoichiometry, three possible surface termination models of as-synthesized PQDs are proposed as shown in Fig. 4. By cutting a idealized cubic $CsPbX_3$ bulk lattice to achieved the upper bound for the X/P ratio. In such a way that Cs and X atoms form the outermost layer of the PQDs, denoted as $[CsPbX_3](PbX_2)\{CsX\}$. This is a relatively common situation. Alternatively, the lower X/Pb bound is given by cutting the QD such that it is terminated with a PbX_2 layer, which corresponds to a structure of $[CsPbX_3](CsX)\{PbX_2\}$ However, in reality, PQDs are always terminated with long, insulating ligands, (OAm and OA) to render them colloidally stable by means of steric repulsion. Thus, experimentally derived PQDs are supposed to have a generic surface structure of $[CsPbX_3](PbX_2)\{CsX'\}$, which corresponds to a $CsPbX_3$ core terminated by a PbX_2 inner shell and an outer shell composed of monovalent cations Cs and anions ($X' = X^-$ and carboxylic acid ligands). This termination completes the

Published on 27 de setembre 2023. Downloaded on 11/2/2026 22:48:11.

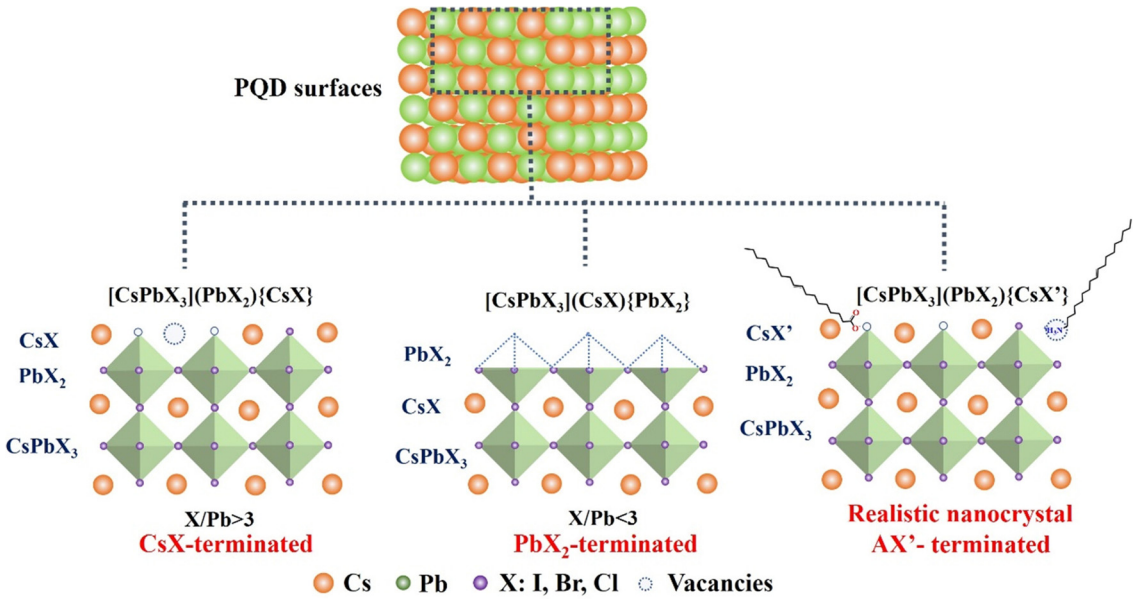

Fig. 4 Idealized surface termination models for the as-synthesized $CsPbX_3$ QDs.

octahedral coordination around the metal and helps reduce the density of midgap states. This result was further proved by Chen *et al.* through high-resolution solid-state NMR spectroscopy characterization.[30] The $CsPbBr_3$ QDs are CsBr terminated (not $PbBr_2$ terminated) with alkylammonium ligands substituting into some surface Cs sites. Therefore, a halogen vacancy is the most abundant defect in PQDs due to the special type of termination.

On the other hand, the surface chemistry of PQD is more complex due to the presence of surface capping ligands.[26] Most often, combinations of long-chain amines with long-chain acids have been used as ligands in the synthesis of colloidal PQDs. One of the most used amine–acid pairs is OA and OAm.[17,21,63–66] They can not only form the PQD dispersion in nonpolar solvent forming a uniform colloidal system, but also efficiently passivate the surface defects of PQDs.[17,21]

However, the ligands of OA and OAm binding to the PQD surface are highly dynamic, and therefore ligands are easily lost during the isolation and purification procedure and thus create enormous amounts of undercoordinated atoms[29,67,68] (Fig. 5).

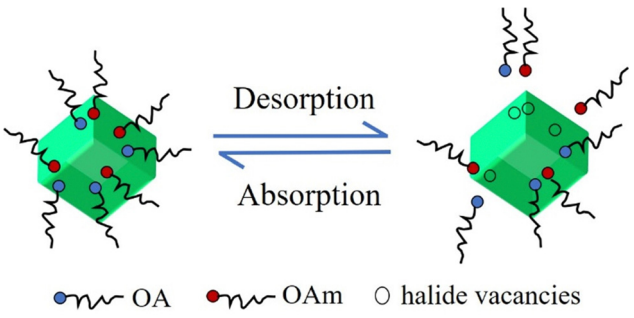

Fig. 5 Schematic representation of the dynamic surface stabilization in $CsPbX_3$ QDs.

The undercoordinated Pb atoms on the PQD surface usually act as charge-trapping centers, thereby inhibiting charge extraction in photovoltaic devices. Therefore, the fine controlling surface chemistry of PQDs is critical for the development of highly efficient and stable PQD solar cells. In this section, we provide a comprehensive discussion of the surface properties of PQDs from the perspective of surface passivation and surface treatment using ligands.

Fig. 6 illustrates the types of passivation ligands used in PQD systems. Ligand detachment from the PQD surface result in the formation of A- and X-site vacancies for charge neutralization. There are mainly two types of approaches for the surface passivation of PQDs: (1) organic ligand modification, and (2) inorganic chemical treatment.

3.1 Organic ligand modification

The highly dynamic binding between PQDs and surface ligands provides the possibility of ligand exchange in the PQDs. Ligand

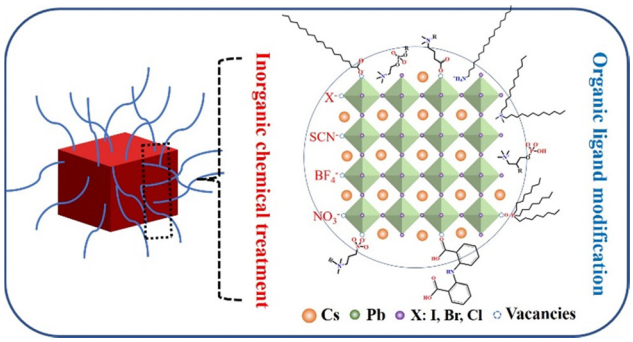

Fig. 6 Schematic illustration of the ligand-capped PQDs and an enlarged view of the nanocrystal surface with defects and different types of surface ligands used for the stabilization of PQDs.

 This journal is © The Royal Society of Chemistry and the Chinese Chemical Society 2024

Published on 27 de setembre 2023. Downloaded on 11/2/2026 22:48:11.

detachment from the surface of PQDs leads to the formation of A-site and X-site vacancies.[67,69–72] The ligand molecules are expected to fill the A-site and X-site vacancies to recover the photoluminescence (PL) of the PQDs.[73,74] The interaction of PQDs with surface ligands can be described according to classification of the covalent bond between surface ligands and PQDs, which is called L-, X-, and Z-type ligands. They are classified by the number of electrons (2, 1, and 0, respectively) provided to the metal by the neutral ligand when it forms a bond with the surface[73,75] (Fig. 7). L-Type ligands usually share a lone electron pair with Pb^{2+} cations acting as Lewis bases such as alkylamine and alkyl phosphine oxide; X-type ligands mainly include alkylammonium salts, alkyl phosphonic/alkyl carboxylic/alkyl sulfonic acids and thiol/thiolate acids oleates; while Z-type ligands accept a lone electron pair from the halide anions acting as the Lewis acids such as CdX_2 or $Cd(CH_3COO)_2$.[73,76,77] Due to the ionic properties, the most common ligands used to cover PQD surfaces fall into the X- and L-type categories.

Though OA/OAm ligands are widely used as native ligands for the synthesis of PQDs, the weak binding between PQD surfaces and ligands usually leads to ligand desorption, resulting in a dramatic decrease in the PLQY and stability of PQDs, and even phase transition. X-Type ligands (cations and anions) have been proven to passivate the A and X sites on the PQD surface well.[29,61,78–81] One of the early studies on the surface passivation of PQDs was reported by Pan *et al.*[78] They demonstrate an air- and photo-stable $CsPbBr_3$ QDs by passivating with didodecyl dimethylammonium sulphide. Because of the robustness of the passivated PQDs, they are used for the development of a perovskite-based device that exhibits ultra-stable amplified spontaneous emission. However, the passivation mechanism at the molecular level is unclear. Later, Pan *et al.*[79] developed a two-step ligand exchange process for passivating $CsPbX_3$ (X = Cl, and Br) with didodecyl dimethylammonium bromide (DDAB) (Fig. 8a). Through the ligand exchange process, DDAB easily attaches to the PQD surface and provides better passivation of the trap states. Thus, the PLQY is increased from 49% to 71%. Compared to those of OA/OAm capped PQDs, the relatively short-chain ligand can promote carrier transport in the fabricated LEDs, which demonstrated much a higher EQE and luminescence intensity. Subsequently, DDAB and its derivatives have been widely used in $CsPbBr_3$ QDs.[82–86] Park *et al.*[84] studied the effect of the bulkiness of quaternary ammonium bromide (QAB) ligands on the properties and stability of $CsPbBr_3$ QDs. The less bulky QAB ligands surrounded the surface of QDs effectively, and brought better surface passivation and less aggregation compared to bulky QAB ligands, and finally the optical property and stability of $CsPbBr_3$ QDs were enhanced. Following these studies, various ligands have been reported for the electronic passivation of PQDs to improve their optical properties.[29,66,73,80,87–89]

For cubic phase $CsPbI_3$, it is very sensitive and can be easily converted to an orthorhombic phase ("yellow" phase) under ambient conditions.[17,21,90] In Wang's work,[91] an alkyl phosphonic acid, bis-(2,2,4-trimethylpentyl) phosphinic acid (TMPPA), is used as a replacement of OA in the synthesis of $CsPbI_3$ QDs while its mechanistic binding is concealed. Unlike OA, TMPPA and its ion pairs do not bind to the surface of PQD while OAm species dominate. A better understanding of the deeper mechanisms is needed for the future. Considering the unstable nature of $CsPbI_3$ QDs, the ligand 2,2′-iminodibenzoic acid (IDA) was introduced using a post-synthetic method[66] (Fig. 8b). Due to the much stronger binding between $CsPbI_3$

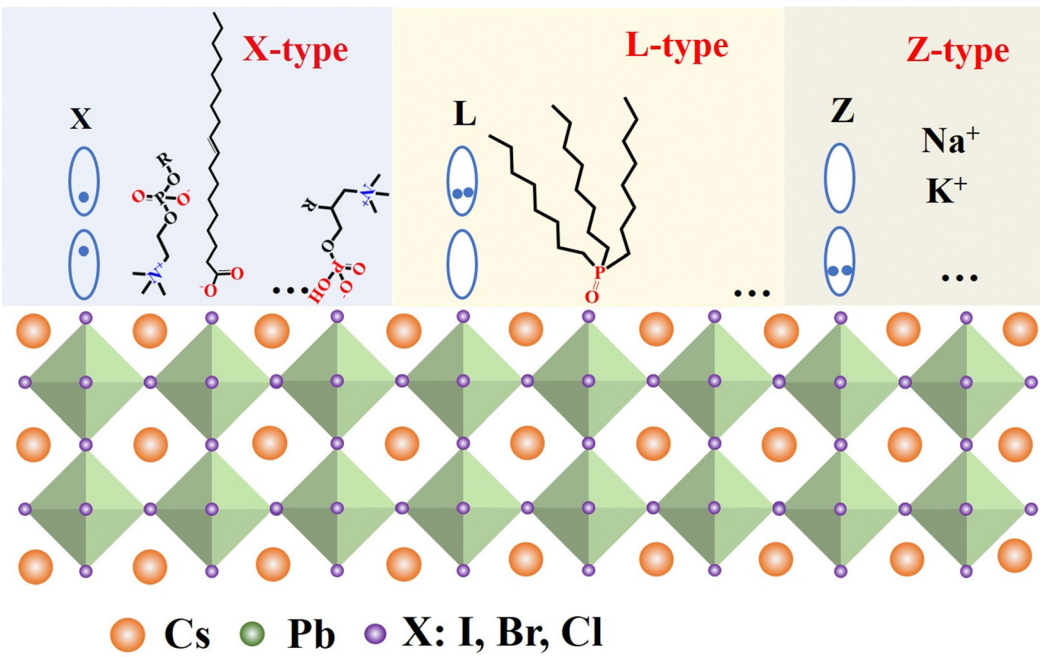

Fig. 7 PQD ligand-binding motifs according to the covalent bond classification method.

Published on 27 de setembre 2023. Downloaded on 11/2/2026 22:48:11.

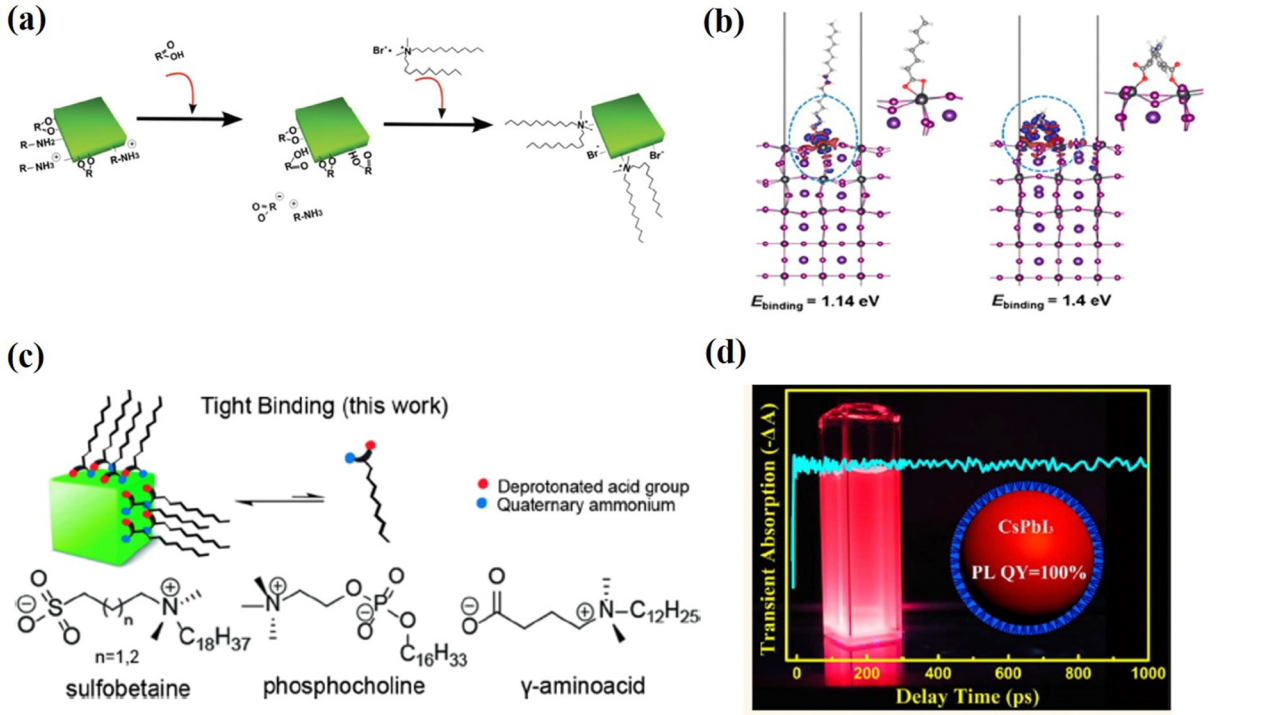

Fig. 8 (a) The ligand–exchange mechanism on $CsPbBr_3$ QD surfaces. Reproduced with permission from ref. 79. Copyright 2016, Wiley-VCH. (b) DFT calculations of charge redistributions for OA and IDA passivated PQD surfaces. Reproduced with permission from ref. 66. Copyright 2018, American Chemical Society. (c) Several zwitterionic capping ligands for improving the chemical durability of PQDs. Reproduced with permission from ref. 92. Copyright 2018, American Chemical Society. (d) Photos of TOP-prepared $CsPbI_3$ QDs with high PLQYs. Reproduced with permission from ref. 96. Copyright 2017, American Chemical Society.

QDs and IDA compared to OA, the PQDs with IDA treatment display a PLQY of more than 95% and a slightly improved lifetime, indicating a reduction in the surface trap state by passivation.

Another family of X-type ligands that has received much attention is zwitterionic (or bidentate) ligands, in which the two functional groups with negative and positive charges simultaneously bind to the X-site and A-site, respectively.[61,62,92–94] The long-chain zwitterionic ligands include sulfabetaine, phosphocholine, and γ-amino acid92 (Fig. 8c). In each molecule, both the deprotonated acid group and the quaternary ammonium are tightly bound to the PQDs by the chelating effect. More importantly, the cationic and anionic groups in the zwitterionic molecules prevent external neutralization, so that the PQDs are not surrounded by the insulating molecules and the charge transportation is improved. Furthermore, due to the chelating effect, these ligands bind much more strongly to the PQD surface and the resulting PQDs exhibit long-term stability and a high PLQY even after different solvent washes. A similar passivation effect was achieved by post-treating PQDs with short-chain zwitterionic 2-aminoethanethiol (AET)[95] with both amine and thiolate groups, further verifying the synergistic functions of zwitterionic ligands. This novel class of ligands may be promising candidates for the synthesis of these PQDs in future applications.

As aforementioned, X-type ligands have mostly been used for passivation of the A and X sites of the PQD surface. The relatively soft L-type Lewis bases are also considered attractive alternative ligands with excellent passivation effects because they have a much stronger affinity for lead cations on PQD surfaces than carboxylate ligands.[96–102] Liu *et al.*[96] used TOP to synthesize the $CsPbI_3$ QDs. Highly luminescent and stable $CsPbI_3$ QDs were obtained by forming stable and reactive TOP-PbI_2 precursors. The PLQY of all samples of different sizes prepared by the TOP-PbI_2 precursor system reached 100%, indicating the complete elimination of surface defects (Fig. 8d). In addition, the TOP-based PQDs retain more than 85% PLQY after storage for one month. Alpert *et al.*[99] reported another promising molecule, tributyl phosphine (TBPh), for passivation of $CsPbX_3$ QDs. The post-treatment with TBPh improves the PLQY of $CsPbBr_3$ up to 100% and leads to superior surface passivation towards $CsPbX_3$ films. Trioctylphosphine oxide (TOPO) was also reported to passivate and stabilize $CsPbX_3$ QDs even in the presence of the polar solvent ethanol.[98]

Other L-type ligands with sulfur functional groups such as sulfonic acids, thiolates or thioethers are also used to improve stability and enhance luminescent properties due to their strong interaction with Pb^{2+} ions.[103] The $CsPbBr_3$ QDs prepared using dodecyl benzene sulfonic acid (DBSA) exhibited a PLQY up to 90%, which was retained for more than five months of storage, thereby showing a remarkable enhancement of stability.

3.2 Inorganic chemical treatment

Surface passivation can be achieved not only by covering the surface with protective organic ligands, but also by changing

 This journal is © The Royal Society of Chemistry and the Chinese Chemical Society 2024

Published on 27 de setembre 2023. Downloaded on 11/2/2026 22:48:11.

the surface state using post-treatment with inorganic chemicals. Unlike PQDs with chain ligands bound to lead or halide ions on the surface, chemical-specific post-treatments can remove excess ions, adjust the composition, and repair shallow traps on the surface, thereby improving their optical properties.

Many reports have shown that halide-rich surfaces favor desirable optical properties.[29,59,61,104] To build up a halide-rich surface, different metal halide salts have been used to control the defects and optical properties of these PQD surfaces. $PbBr_2$ and $ZnBr_2$ are the most effective among several metal bromide salts ($PbBr_2$, $ZnBr_2$, $InBr_3$, $CuBr_2$, AgBr) as an excellent bromide donor in enhancing the PLQY of $CsPbBr_3$ PQDs.[61,89,105–111] The Konstantatos group[94] obtained a near-unity PLQY for $CsPbBr_3$ QD films post-treated with $PbBr_2$. The addition of $PbBr_2$ which dissolved in both an amine and a carboxylic acid to the as-prepared PQDs induced strong ligand binding at the surface and introduced an excess of Br^-. These two effects essentially promote surface defect passivation and, consequently, result in a substantial enhancement of the PLQY. Bohn *et al.*[108] investigated the mechanism of $PbBr_2$ passivation through post treatment. The high PLQYs were achieved through post-synthetic treatment of the $CsPbBr_3$ nanoplate dispersions with $PbBr_2$-ligand addition (Fig. 9a). Time-resolved photoluminescence (TRPL) spectroscopy and differential transmission spectroscopy (DTS) revealed that the addition of $PbBr_2$ repairs Br and Pb vacancies on the surface rather than internal traps. The much stronger radiative recombination also further demonstrates the removal of surface defects.

In addition, metal halide treatment was found to be very effective in improving the PLQY of weakly emitting $CsPbCl_3$ QDs. Due to the mid-gap traps of Cl-deficient surfaces, the Cl-based PQDs generally suffer from extremely low PLQYs. To overcome such issues, a trivalent metal chloride salt (YCl_3)[109] was introduced to passivate the surface defects of $CsPbCl_3$ QDs and increase the PLQY up to 60% (Fig. 9b). The authors proposed that YCl_3 robustly fill the Pb–Cl ion pair defects and passivate the uncoordinated Pb atoms on the QD surface. An in-depth investigation of how the Y^{3+} ions are doped in the $CsPbCl_3$ PQDs is further needed. Similarly, Mondal *et al.*[110] reported that post-treatment of $CsPbCl_3$ QDs with $CdCl_2$ at room temperature leads to an increase in PLQY from 3% to 98%. This enhancement is due to the substitution of Pb^{2+} by Cd^{2+} ions during the cation exchange process.

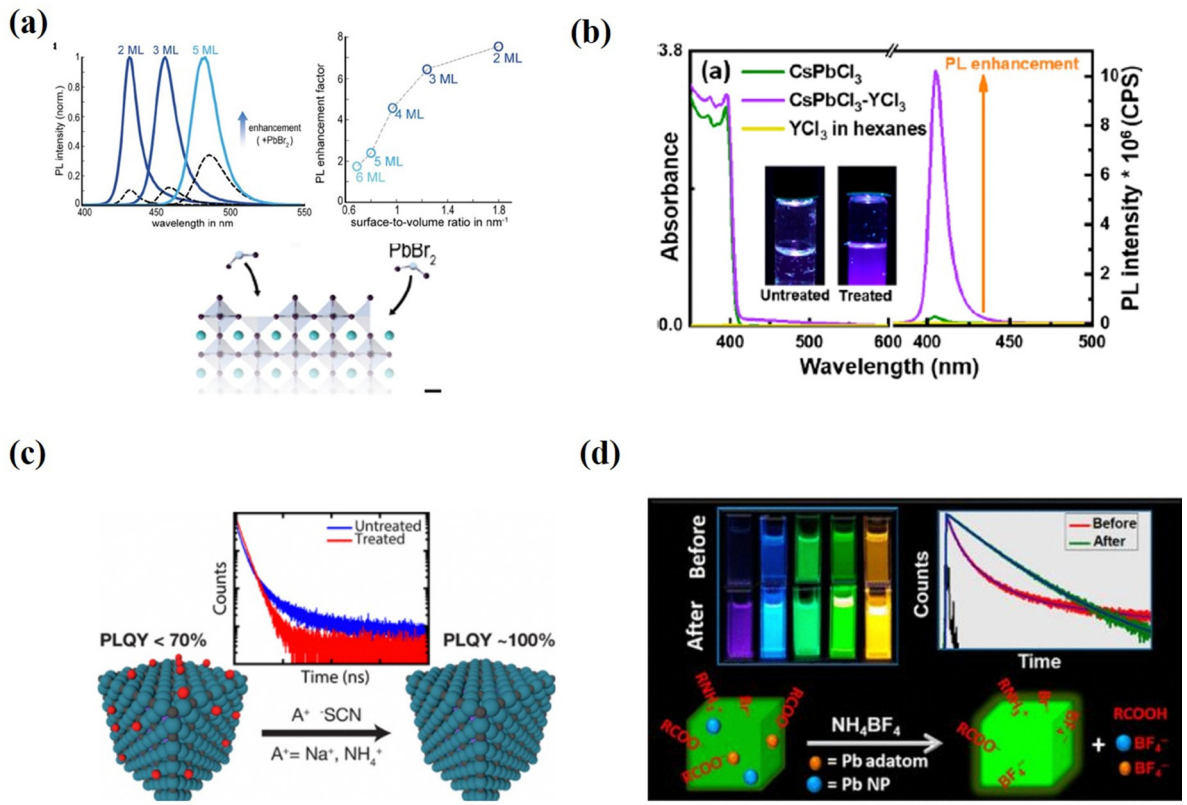

Fig. 9 (a) PL spectra of the initial samples (dashed lines) and samples treated with $PbBr_2$ (solid lines) (left) and the enhancement factor as a function of layer number (right), and an illustration of the defects fixed with $PbBr_2$ on the surfaces of nanoplates. Reproduced with permission from ref. 108. Copyright 2018, American Chemical Society. (b) Steady-state optical absorption and PL spectra for the as-synthesized $CsPbCl_3$ QDs dispersed in hexanes before and after YCl_3 surface passivation; the insets are photographs of the untreated and YCl_3-treated QDs under 365 nm UV illumination. Reproduced with permission from ref. 109. Copyright 2018, American Chemical Society. (c) Schematic illustrations of thiocyanate post-treatment for essentially trap-free PQDs. Reproduced with permission from ref. 112. Copyright 2017, American Chemical Society. (d) Schematic illustrations of tetrafluoroborate post-treatment for essentially trap-free PQDs. Reproduced with permission from ref. 113. Copyright 2018, American Chemical Society.

Published on 27 de setembre 2023. Downloaded on 11/2/2026 22:48:11.

Not limited to the Pb or halide reagents mentioned above, a post-synthetic thiocyanate (SCN^-) surface treatment strategy was introduced by Koscher *et al.*[112] to remediate the lead-rich surface.

Thiocyanate treatment deactivated the surface traps of both fresh (~92% PLQY) and aged (~63% PLQY) $CsPbBr_3$ PQDs, and the treated samples showed a near-uniform PLQY and high stability. The stoichiometric ratio of Pb to Br atoms attained 1 : 3 after removing supernumerary Pb atoms from the PQD surface (Fig. 9c). However, a drawback of this method is that it is not applicable to $CsPbX_3$ with other halide components. Another method was reported by Ahmed *et al.*[113] They used tetrafluoroborate salts to treat the PQDs and the PLQYs of the green emissive $CsPbBr_3$ and blue emissive $CsPbBr_xCl_{3-x}$ are near unity (Fig. 9d). It should be noted that the size and shape of the parent PQDs are preserved in all these post-treatments.

As mentioned above, the undercoordinated lead atoms (in other words, halogen vacancies) are the most abundant active defects in these PQDs and new synthetic strategies employing halide-rich reaction conditions have been developed.[106,114–121] A three-precursor synthesis approach was explored. Three separate reagents are used as independent sources of cesium, lead, and halogen, where the desired lead and halogen ratio can be easily controlled. Liu *et al.*[115] utilized NH_4X (X = Cl, Br, or I) and PbO to substitute for traditional PbX_2 as the separate sources of halides and Pb so that the Pb : X ratio could be adjusted at will for the sake of investigation. In addition, PQDs are synthesized in this halide-rich environment with higher quality and greater durability against environmental changes, like purification treatment for further device fabrication (Fig. 10a). Yassitepe *et al.*[121] further developed the three-precursor approach in order to synthesize OA-capped $CsPbX_3$ QDs by eliminating alkylamines from the synthesis. In a typical reaction, Pb-acetate and Cs-acetate are reacted with quaternary alkylammonium halides, such as tetraoctylammonium halides (TOA-X) for the preparation of OA-capped $CsPbX_3$ PQDs without the need for post-anion exchange methods. It is observed that the absence of OAm significantly accelerated the growth kinetics, thus enabling the synthesis of $CsPbX_3$ QDs at lower temperatures (*i.e.*; 75 °C). The $CsPbBr_3$ QDs obtained by this approach exhibited PLQYs up to 70%, as well as enhanced colloidal stability. This method, however, failed to produce $CsPbI_3$ QDs of similar quality and stability.

For $CsPbI_3$ QDs, the iodine precursor and lead source cannot be easily made independently. Metallic lead particles would be generated due to the reducibility of OA, which worsen the stability and optical properties of $CsPbI_3$ QDs. Therefore, a more effective iodine-rich synthetic route should be developed. Recently, trimethylsilyl iodide (TMSI) has been explored in the synthesis of $CsPbI_3$ QDs.[120] In a typical reaction, a certain amount of TMSI is injected into the mixed solution containing Pb-oleate, Cs-oleate, OA, and OAm. With a TMSI/Pb-oleate molar ratio of ~4.2, the obtained $CsPbI_3$ QDs have excellent storage stability (over 85% of PLQY after 105 days storage) and thermal stability (Fig. 10b). Although the three-precursor approach allows one to use the desired ionic stoichiometry because the halide and metal cation sources are no longer linked, its potential versatility is limited by a number of drawbacks. First, the universality of this approach is not very good. The fact that the synthesis of $CsPbCl_3$ QDs has not yet been reported using this strategy suggests that the halide precursors react poorly under the reaction conditions of this approach. Moreover, the PQDs synthesized using this method are rarely used in the preparation of solar cells.

In the development of all-inorganic perovskites, inert oxide materials have also been regarded as promising protective

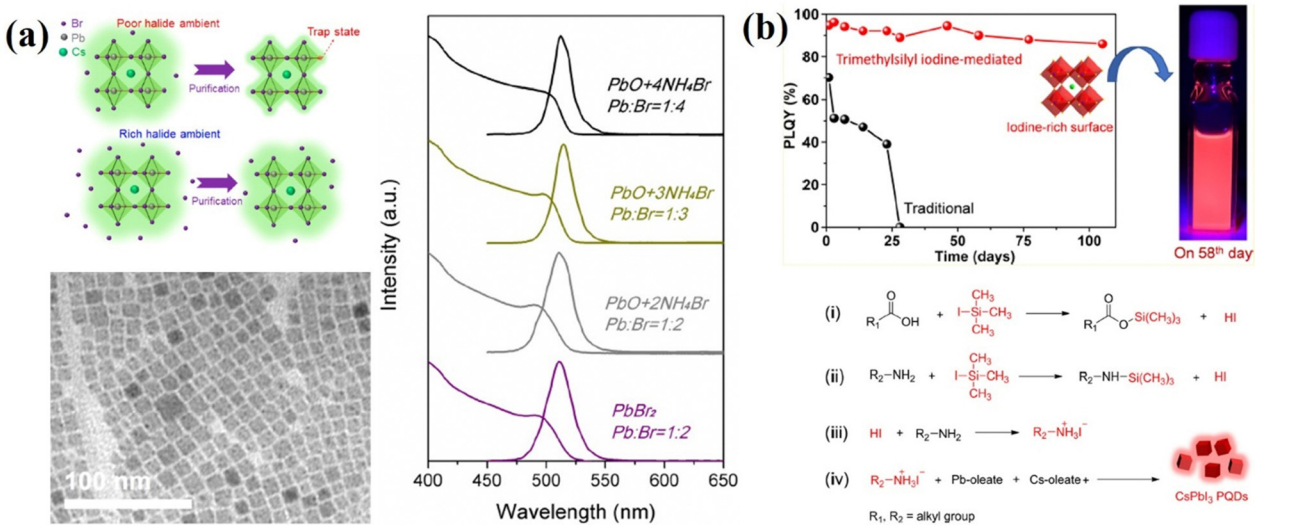

Fig. 10 (a) Schematics for halide-poor and halide-rich circumstances for the synthesis of QDs, TEM images of $CsPbBr_3$ QDs and PL and UV spectra of QDs synthesized in different precursors in different halide circumstances. Reproduced with permission from ref. 115. Copyright 2017, American Chemical Society. (b) PLQYs of TMSI-CPI and Tra-CPI QDs as a function of storage time and reaction mechanism for the TMSI-mediated synthesis of CPI QDs. Reproduced with permission from ref. 120. Copyright 2019, American Chemical Society.

 This journal is © The Royal Society of Chemistry and the Chinese Chemical Society 2024

Published on 27 de setembre 2023. Downloaded on 11/2/2026 22:48:11.

shells for the passivation of $CsPbX_3$ QDs. Due to their high stability and inert properties, oxides mainly including silica (SiO_x) and alumina (AlO_x) have been introduced to stabilize $CsPbX_3$ against polar solvents, heat, light and oxygen.[122–126] For the first time, Loiudice and co-workers[122] assembled $CsPbBr_3$ QDs into an amorphous AlO_x matrix through an atomic layer deposition (ALD) method. The interaction between the AlO_x precursor and $CsPbBr_3$ surface favored the uniform coating and preservation of the excellent optoelectronic properties of perovskite QDs. The Liu group[123] proposed a simple but efficient method to prepare $CsPbX_3$ QDs/SiO_2 nanocomposites in 2016. By directly mixing $CsPbX_3$ nanocubes with mesoporous SiO_2 with pore sizes of 12–15 nm, the nano cubes could be incorporated into the pores of SiO_2 (Fig. 11a). Besides the template-assisted method, *in situ* formation of SiO_2 shells on the surfaces of $CsPbX_3$ QDs has also been studied, (3-aminopropyl) triethoxysilane (APTES) was chosen by Sun *et al.*[124] as both the capping agent for inorganic PQDs and the precursor for a silica matrix as shown in Fig. 11b. As a result, SiO_2 wrapped $CsPbX_3$ crystals were formed, exhibiting significant enhancement of stability in comparison with pure $CsPbX_3$ QDs. Li *et al.*[125] designed mesoporous aminated SiO_2 spheres as the hard templates, which could act as the reaction platforms and adsorption sites for $CsPbBr_3$ QDs as shown in Fig. 11c. The QDs/aminated-SiO_2 composites exhibited a 7-fold increase in PL intensity compared with neat $CsPbBr_3$ QDs. Subsequently, various methods were developed to grow SiO_2 shell layers to enhance the photovoltaic properties and stability of $CsPbX_3$ QDs. Recently, Rossi *et al.*[126] used the anhydride-mediated transformation of Cs_4PbBr_6 into $CsPbBr_3$ QDs for the preparation of $CsPbBr_3$@SiO_2 core–shell (Fig. 11d). The $CsPbBr_3$@SiO_2 nanocrystals exhibited increased stability in ethanol by retaining 95% of their initial PL intensity after 9 days of immersion in ethanol. Although this core–shell structure plays a large role in the stabilization of $CsPbX_3$ QDs, the outer shell is generally inert and hinders charge transfer between QDs. Therefore, the application of this core–shell structure in quantum dot solar cells will be limited.

In summary, various types of ligands have been used in the synthesis of PQDs. In most studies, it is shown that the passivating ligands help to improve the PLQY as well as the stability of PQDs. However, the most frequently used ligands for PQDs used in solar cells have been limited to long-chain OA/OAm. The use of other ligands should be investigated to enhance the optoelectronic properties and stability of PQDs toward efficient and stable photovoltaic devices.

4. Surface engineering of PQD solar cells

When applying PQDs in solar cells, surface chemistry plays a critical role in determining the device performance. Specifically, organic long-chain ligands (OA and OAm) are widely adopted to impart PQDs with the desired mono-dispersity and stability.[17,21,26] However, these insulating organic ligands hinder the transfer of charge carriers from dot-to-dot. Abundant studies have shown that replacing long-chain ligands with

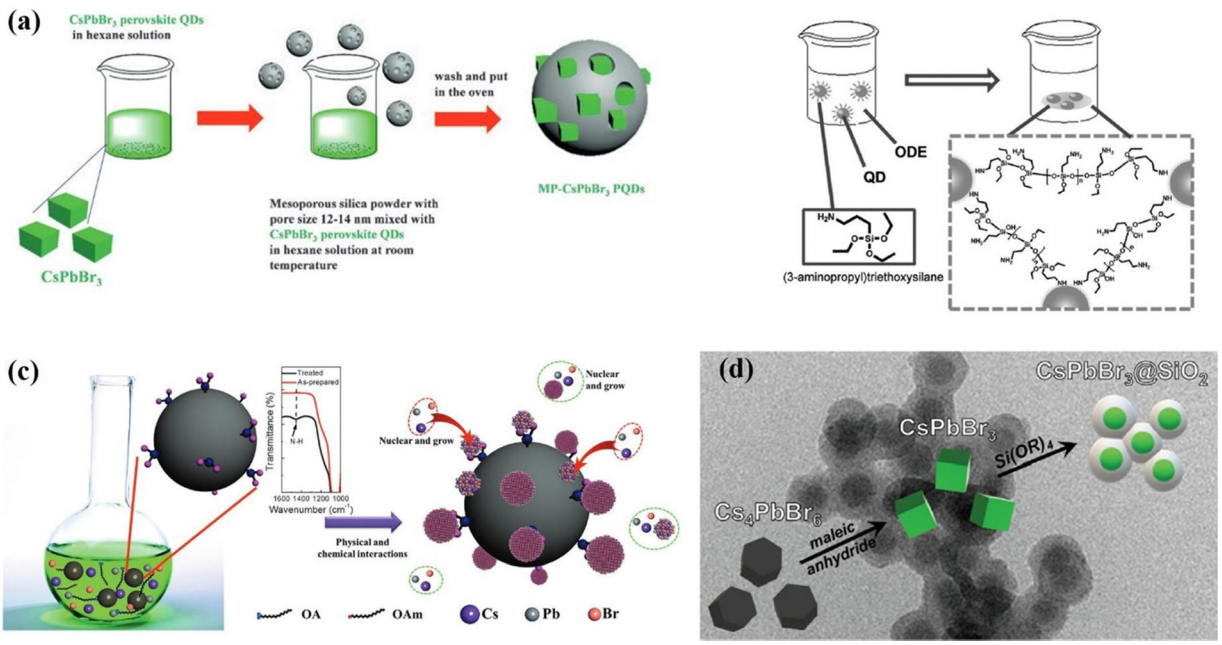

Fig. 11 (a) The synthesis process of mesoporous silica green PQD nanocomposites. Reprinted with permission from ref. 123. Copyright 2016 Wiley-VCH. (b) Schematic illustration of the formation of QD/silica composites. Reprinted with permission from ref. 124. Copyright 2016 Wiley-VCH. (c) Schematic illustration of the synthetic strategy and fabrication of perovskite/A-SiO_2. Reprinted with permission from ref. 125. Copyright 2017 Wiley-VCH. (d) The process starts from Cs_4PbBr_6 QDs that are converted into $CsPbBr_3$@SiO_2 QDs. Reprinted with permission from ref. 126. American Chemical Society.

Published on 27 de setembre 2023. Downloaded on 11/2/2026 22:48:11.

shorter ones can significantly improve the performance of PQD solar cells.[17,70,127] It should be noted that the removal of the long insulating ligands on the surface of PQDs may result in surface defects, phase transition, and degradation of the PQDs, so that re-passivation of the PQD surface is needed. Therefore, it is important to study the PQD surface engineering as well as their impact on the photovoltaic performance of PQD solar cells. We present this part from two aspects, one is the surface ligand engineering and the other is the passivation of defects resulting from ligand removal.

4.1 Surface ligand engineering

Ligand bonding to the surface of PQDs is a double-edged sword. On one hand, ligands not only make the PQDs in a nonpolar solvent forming a colloidal system, but also efficiently passivate the surface defects of PQDs.[17,21,96,128] On the other hand, long, insulating ligands trap charges inside the PQDs and increase the interparticle distance, resulting in poor electronic coupling.[17,127] Therefore, to improve the conductivity of PQD solid films, the original long-chain ligands are always replaced by shorter ones through solid-state or liquid-state ligand exchange as shown in Fig. 12.

4.1.1 Solid-state ligand exchange. The film fabrication procedure of current PQD solar cells is mostly based on a layer-by-layer method that has been widely employed in QD solar cells.[17,129] In order to prepare PQDs for utilization in solar cells, the PQDs must be washed to remove excess unreacted precursors. Methyl acetate (MeOAc) has been demonstrated as a suitable antisolvent that can precipitate the PQDs without inducing agglomeration or phase transition during the purification process.[17] Furthermore, MeOAc is used again in PQD film preparation. The PQD film is swiftly dipped in $Pb(OAc)_2$ or $Pb(NO_3)_2$ saturated MeOAc and then rinsed with neat MeOAc to partially remove the long-chain ligands. The film is used to fabricate solar cells with the device architecture of FTO/TiO_2/$CsPbI_3$ QDs/spiro-OMeTAD/MoO_3/Al. A large open-circuit voltage of 1.23 V and an efficiency of 10.77% were achieved (Fig. 13a). While acetate replaces oleate ligands as described above, cationic ligands (OAm^+) are found to remain in the PQD films after the MeOAc treatment[130] (Fig. 13c).

In order to further improve the carrier mobility of $CsPbI_3$ QD arrays, Sanehira *et al.*[127] applied AX salt to treat the prepared $CsPbI_3$ QDs films (Fig. 13b). When formamidinium iodide (FAI) is used, the smaller FA^+ replaces long-chain OAm^+ on the PQD surface. They achieved an impressive carrier mobility boosting from 0.23 to 0.50 $cm^2\ V^{-1}\ s^{-1}$ and the corresponding current density (J_{SC}) increases from 9.22 to 14.37 mA cm^{-2} with a target PCE of 14.3%. However, during ligand exchange, MeOAc hydrolysis results in the formation of intermediate substances acetic acid and methanol. Lead halide perovskites decompose significantly under acidic conditions including protons and polar media. Therefore, proton and solvent polarity should be minimized during the ligand exchange process.[106,131–135] Kim *et al.*[136] replaced the Pb-based ionic salts with NaOAc to generate OAc^- directly (Fig. 13d), avoiding the formation of surface trap states and achieving a J_{SC} value of 15.21 mA cm^{-2} in $CsPbI_3$ QD solar cells. Although FAI post-treatment has proven to be an effective method for improving charge transport, the removal of hydrophobic OAm leads to easy penetration of water, which accelerates the transformation of the cubic phase to the yellow orthorhombic phase. In addition, FAI post-treatment is sensitive to reaction time and hybridizes the fully inorganic $CsPbI_3$ QDs with organic FA cations on the surface and inside of the PQDs.[127] Therefore, phenethyl-ammonium (PEA) cations were introduced to post-treatment $CsPbI_3$ QDs films by Kim *et al.*[137] The PEA group is an aromatic organic cation with a larger size than the Cs^+ cation, which can effectively prevent the phase decomposition of perovskite materials caused by water molecules. The PEA groups successfully replace the OAm ligand on the PQD surface, thus greatly improving the electronic coupling between the dots (Fig. 13e). Finally, PEA-incorporated $CsPbI_3$ QD solar cells show a high PCE of 14.1% and high moisture stability, maintaining more than 90% of the initial performance after 15 days under ambient conditions. Recently, Jia *et al.*[138] demonstrated an efficient solvent-mediated ligand exchange of PQDs. Considering the dielectric constant and acidity, 2-pentanol was screened as an ideal solvent of short ligands for the post-treatment of PQD solid films to sufficiently remove pristine insulating OAm ligands from the PQD surface without introducing halogen vacancy defects, thereby improving the charge carrier transport within the PQD solid films (Fig. 13f). As a result, by using 2-pentanol as the solvent and Cl as the short ligand for the post-treatment of PQD solid films, the PQD solar cell yielded a PCE of 16.53% (Fig. 13g), which is the highest value obtained among inorganic PQD solar cells.

The ligand exchange process mentioned above is generally a two-step ligand exchange. In the first step of ligand exchange, the OA ligand is replaced by acetic acid produced by MeOAc hydrolysis, forming PQD surface-bound acetate and free OA.[17] The second-step ligand exchange was performed using FAI to replace the OAm ligand on the PQD surface.[127,130] FAI post-treatment is sensitive to reaction time due to the small cation miscibility activation energy (0.65 eV) between FA^+ and Cs^+ in PQDs, the cation exchange will occur in the primitive $CsPbI_3$ PQDs, forming orthorhombic-phased $Cs_xFA_{1-x}PbI_3$ bulk film, significantly lowering the photovoltaic performance of PQD solar cells.[139,140] Therefore, a single-step ligand exchange

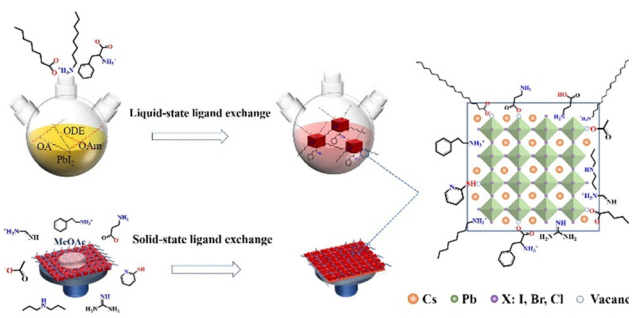

Fig. 12 Schematic illustrations of ligand exchange in two ways, liquid-state ligand exchange or solid-state exchange.

 This journal is © The Royal Society of Chemistry and the Chinese Chemical Society 2024

Published on 27 de setembre 2023. Downloaded on 11/2/2026 22:48:11.

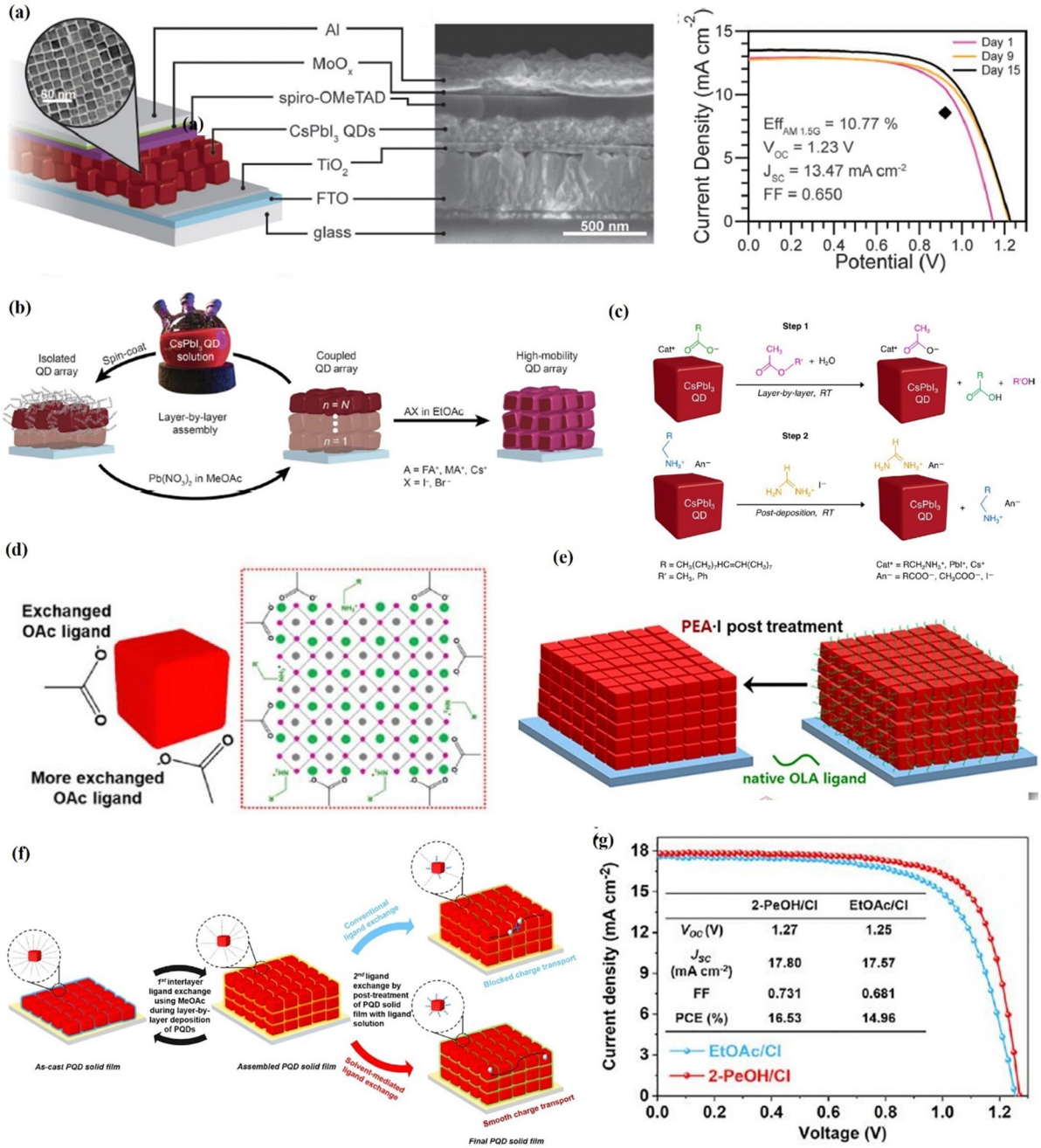

Fig. 13 (a) Schematic (with the TEM image of QDs) and SEM cross-section of the $CsPbI_3$ PQD solar cell and current density–voltage curves of a device measured in air over the course of 15 days. Reproduced with permission from ref. 17. Copyright 2016, American Association for the Advancement of Science. (b) Schematic of the film deposition process and AX salt post-treatment. Reproduced with permission from ref. 127. Copyright 2017, American Association for the Advancement of Science. (c) Ligand exchange process and element analysis of $CsPbI_3$ PQD solid films. Reproduced with permission from ref. 130. Copyright 2018, American Chemical Society. (d) Conventional ligand exchange mechanism based on the hydrolysis of MeOAc and NaOAc-assisted ligand exchange for the direct generation of OAc ions without forming protons and hydroxyl groups. Reproduced with permission from ref. 136. Copyright 2019, Elsevier. (e) Schematic illustrations showing the solid-state ligand exchange process of $CsPbI_3$-QDs to replace OA and OAm ligands with Ac anions and A cations (A = FA, PA, BA and PEA), respectively. Reproduced with permission from ref. 137. Copyright 2020, Elsevier. (f) Post-treatment of PQD solid films, including conventional ligand exchange within EtOAc and solvent-mediated ligand exchange. (g) *J*–*V* curves of EtOAc/Cl- and 2-PeOH/Cl-based PQD solar cells from ref. 138. Copyright 2022, Cell Press.

strategy was reported by Jia *et al.*[141] The amino acids (glycine), which are used as a dual-passivation ligand, could simultaneously passivate the A-site (cesium) and iodine vacancies on the PQD surface, thus improving the defective passivation of PQDs (Fig. 14a). For the photovoltaic applications of the PQDs with improved defect passivation, a high PCE of 13.66% is obtained for the glycine-based PQD solar cells. Moreover, this ligand exchange strategy also avoided using time-sensitive FAI

Published on 27 de setembre 2023. Downloaded on 11/2/2026 22:48:11.

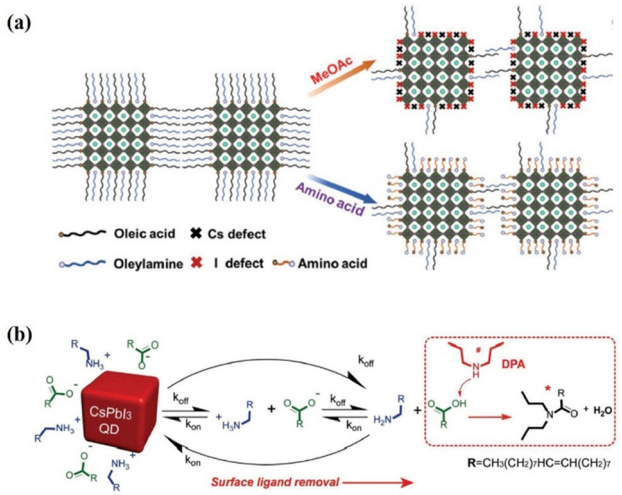

Fig. 14 (a) Schematic illustration of the changes on the PQD surface with conventional MeOAc rinsing and dual-passivation ligands before and after ligand exchange. Reproduced with permission from ref. 141. Copyright 2020, Wiley-VCH. (b) Schematic representation of the PQD dynamic surface stabilization and the ligand removal process assisted by DPA. Reproduced with permission from ref. 142. Copyright 2020, Wiley-VCH.

post-treatment. In addition, a broad variety of amines have already been evaluated using ligand exchange, in which most of the secondary amines (specially di-*n*-propylamine, DPA) improved the performance compared with the control device. The DPA additive can efficiently remove long insulating surface ligands of OA and OAm, even for under-purified PQDs with a high ligand density[142] (Fig. 14b). As a result, the electronic coupling between PQDs is enhanced, leading to improved charge transport, reduced carrier recombination, and a high PCE approaching 15% for $CsPbI_3$ PQD solar cells.

Purification of the synthesized PQD and the deposition of antisolvent-assisted PQD solid films also create a large number of surface vacancies, leading to non-radiative recombination in the PQDs and significantly hindering the performance of the solar cell.[29,67] Ling *et al.*[143] reported a facile surface passivation method for $CsPbI_3$ QD film by adopting a variety of cesium salts (cesium acetate (CsAc), cesium idodide (CsI), cesium carbonate (Cs_2CO_3), and cesium nitrate ($CsNO_3$)). Post-treatment with the Cs-salts not only fill atomic vacancies on the $CsPbI_3$ QD surface but also improve electronic coupling between $CsPbI_3$ QDs (Fig. 15a). The CsAc treated PQD films exhibit improved carrier mobility and reduced trap-assisted non-radiative recombination. Thanks to the improved defect passivation and electronic coupling between dots, the final PCE is 14.10% with an improved J_{SC} of about 15 mA cm^{-2} and V_{OC} of about 1.25 V. Compared with bulk inorganic perovskite solar cells, PQD solar cells show a lower photocurrent density, likely due to the poor carrier transport in the PQD solid films.[144–150] Therefore, further increasing charge extraction is a crucial point to enhance the efficiency of PQD solar cells. Lin *et al.*[151] introduced guanidinium thiocyanate (GASCN) to treat the $CsPbI_3$ QD film, followed with a mild thermal annealing process (called the "LE-TA" strategy). The GA^+ cations adsorb on the PQD surface to replace original amine ligands and fill surface defects during the post-treatment of PQDs (Fig. 15b). Consequently, the GA-matrix-confined $CsPbI_3$ QDs exhibit remarkably enhanced charge mobility and carrier diffusion length, leading to a champion PCE of 15.21% when assembled in photovoltaic devices. Meanwhile, the "LE-TA" method also functioned well in other PQD solar cells like $CsPbBr_3$ and $FAPbI_3$ QDs.

Using a Lewis base has been demonstrated as an effective method to passivate undercoordinated Pb^{2+} in previous reports.[152–156] Lewis bases can provide a pair of non-bonded electrons to coordinate and passivate with the coordinated Pb^{2+} or Pb clusters to form Lewis adducts. Recently, a Lewis base (*para*-mercaptopyridine, 4-MP) was introduced into $CsPbI_3$ QDs *via* post-treatment by Khan *et al.*[157] Both a nitrogen (N) atom and thiol group (–SH) were confirmed to form bonding with the $CsPbI_3$ PQD surface (Fig. 15c). The 4-MP passivated $CsPbI_3$ PQDs exhibit enhanced electronic coupling and fewer trap states, leading to an efficiency of 14.25% for $CsPbI_3$ PQD solar cells. Multidentate molecules, ethylene diamine tetra acetic (EDTA), were introduced to $CsPbI_3$ QD by Chen *et al.*[158] EDTA not only peel the suspended Pb^{2+} ions from the PQD surface but also passivate the surface defects of PQDs by occupying the I^- vacancies (Fig. 15d). By regulating the surface properties, the EDTA-based device yielded a PCE of up to 15.25%.

The application of wide-bandgap $CsPbBr_3$ perovskite in high open circuit voltage solar cells has received great attention in recent years, and it has been applied as the top cell in tandem solar cells.[159–162] $CsPbBr_3$ nanocrystals of 20 nm size synthesized by room temperature reprecipitation have been used in solar cells, delivering a PCE of 5.42% and a V_{OC} of 1.54 V[163] However, the $CsPbBr_3$ inks exhibited poor dispersibility in industrially friendly solvents like hexane, which is detrimental to film uniformity and device reproducibility. The QDs prepared by the hot injection method are well dispersed and are more often used as a photoactive layer. Cho *et al.*[164] investigated the effect of carboxylic acid esters with different alkyl chain lengths, such as methyl acetate, ethyl acetate, propyl acetate, and butyl acetate (BuOAc), on the ligand exchange in $CsPbBr_3$ QD films (Fig. 16a). The results show that the mixed EtOAc/BuOAc solvent with a volume ratio of 8/2 enabled efficient ligand exchange of $CsPbBr_3$ QDs and improved the photovoltaic performance in $CsPbBr_3$ QD solar cells up to a PCE of 4.23% and a V_{OC} of 1.59 V. In addition, a simple and efficient post-treatment method was reported by Zhang *et al.*[165] to remove the long-chain insulating ligand and passivate the QD surface using GASCN salt during the fabrication of $CsPbBr_3$ QD solar cells (Fig. 16b). The device showed a champion PCE of 5.01%. Although high values of V_{OC} have been achieved for $CsPbBr_3$ QD devices, their J_{SC} is still unsatisfactory. In order to further improve the carrier transport of $CsPbBr_3$ QDs, Wang *et al.*[166] applied benzoic acid (BA) to treat $CsPbBr_3$ QD film as shown in Fig. 16c. BA post-treatment was demonstrated to effectively exchange the long-chain ligands and improve the carrier transport of $CsPbBr_3$ QDs, leading to a champion PCE of 5.46% and an improved J_{SC} of 4.84 mA cm^{-2}. Recently, an anion modification strategy was developed to inhibit methanol

Published on 27 de setembre 2023. Downloaded on 11/2/2026 22:48:11.

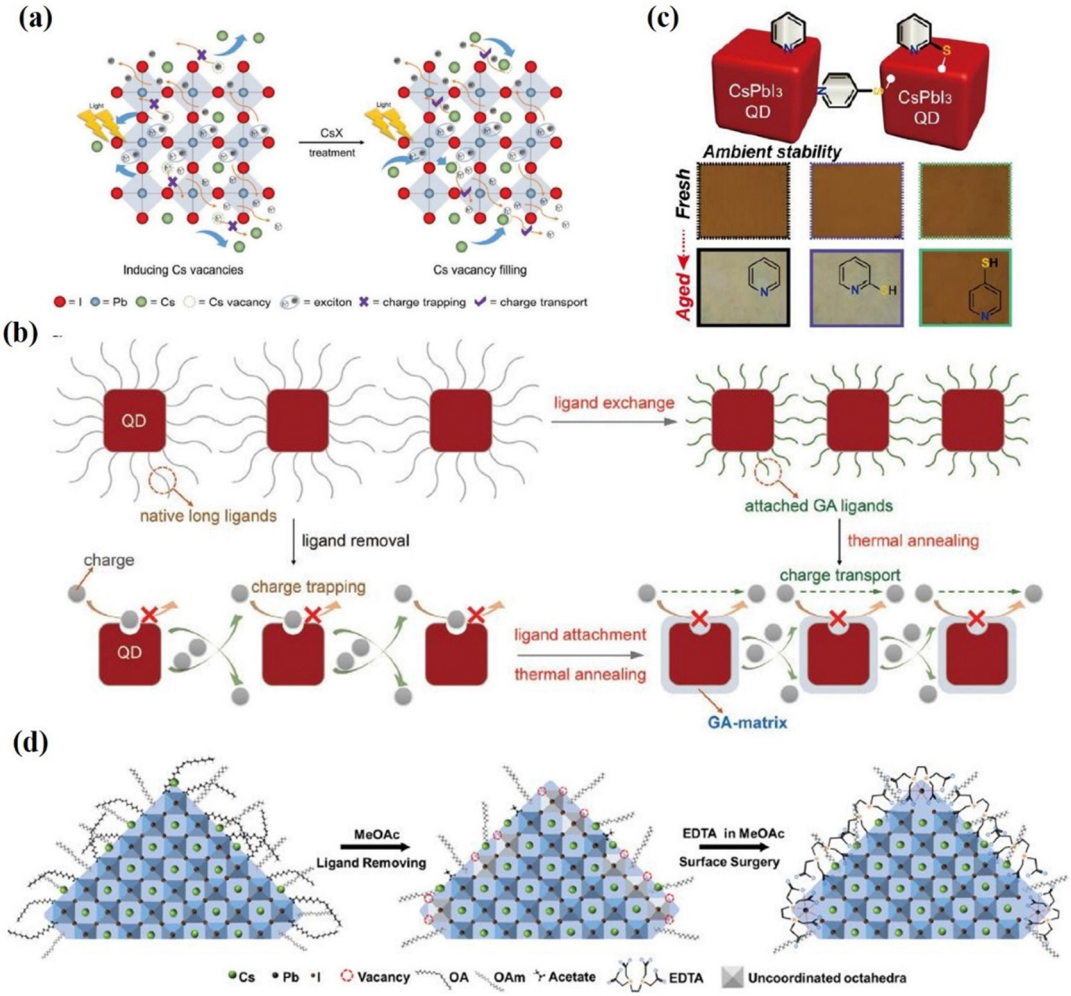

Fig. 15 (a) Schematic illustrations of $CsPbI_3$ QD film deposition and CsX post-treatment process and internal exciton generation, charge trapping, and transport process after ligand removal and Cs-salt post-treatment. Reproduced with permission from ref. 143. Copyright 2019, Wiley-VCH. (b) Schematic diagrams of the formation process of GA-matrix-capped $CsPbI_3$ QD solids *via* the ligand exchange process followed by thermal annealing ("LE-TA" method) induced by GASCN. And its effect on charge transport. Reproduced with permission from ref. 151. Copyright 2020, Wiley-VCH. (c) Stability of the $CsPbI_3$ QD film based on MeOAc treatment (control) and 2-MP and 4-MP post-treatment. Reproduced with permission from ref. 157. Copyright 2020, American Chemical Society. (d) Schematic diagram of the surface surgery treatment of PQDs using EDTA molecules. Reproduced with permission from ref. 158. Copyright 2022, Elsevier.

(MeOH) adsorption on the surface of $CsPbBr_3$ QDs,[135] which was implemented through incorporating a series of guanidinium salts containing different anions (GuaBr, GuaSCN, GuaAc) into each layer of $CsPbBr_3$ QD films. All anions play a positive role in inhibiting the adsorption of MeOH on the QD surface, facilitating charge transfer between perovskite QDs and passivating the defects (Fig. 16d). The GuaAc-based devices deliver a PCE of 7.04%, which is the highest value among inorganic $CsPbBr_3$ QD solar cells.

In short, the solid-state ligand exchange of PQD films through post-treatment provides more possibilities for device optimization. Unlike the complex environment in which colloidal PQDs are found, it is easier to control the surface regulation of the PQD solids without destroying the crystal structure by causing aggregation. However, its potential versatility is limited by a series of disadvantages. The amount of these molecules added and the post-treatment time is limited to a small range, which makes the reproducibility of this treatment relatively poor.

4.1.2 Liquid-state ligand exchange. Besides the solid-state ligand exchange, ligand control during synthesis can also improve the device performance, *via* ligand length reduction and ligand density management. The direct exchange of OAm and OA parts into shorter molecules such as octylamine (OctAm) and octanoic acid (OctAc) during the synthesis process, reduces the insulating barrier for charge exchange in deposited PQDs.[167] That is, the photogenerated charge is easily transferred between PQDs in deposited films made by spin coating or spraying. Indeed, ligands with shorter chains have also been shown to be a better choice for improving charge transfer in conventional chalcogenide QDs,[168] demonstrating the results obtained for PQD.

Published on 27 de setembre 2023. Downloaded on 11/2/2026 22:48:11.

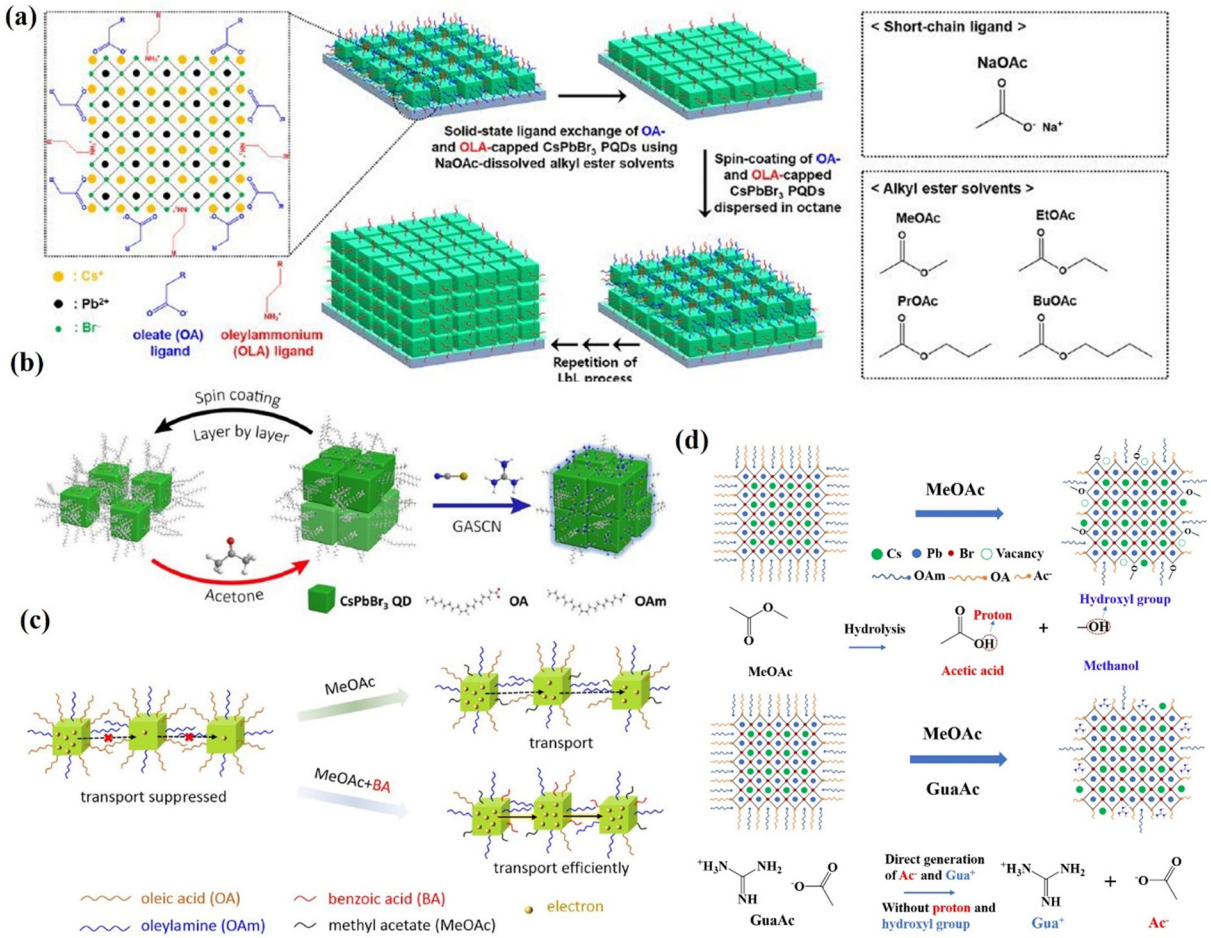

Fig. 16 (a) Schematic of the solid-state ligand–exchange process of $CsPbBr_3$ QDs using NaOAc-dissolved carboxylate ester solutions such as MeOAc, EtOAc, PrOAc, and BuOAc. Reprinted with permission from ref. 164. Copyright 2020 American Chemical Society. (b) Schematic of $CsPbBr_3$ QD film deposition and solid-state post-treatment using different strategies. Reprinted with permission from ref. 165. Copyright 2020 American Chemical Society. (c) Schematic of the effect of MeOAc and MeOAc + BA treatments on the number of long-chain ligands and charge transport of $CsPbBr_3$ QD films. Reprinted with permission from ref. 166. Copyright 2022 American Chemical Society. (d) GuaAc-assisted ligand exchange for the direct generation of Ac ions without forming protons and hydroxyl groups. Reprinted with permission from ref. 135. Copyright 2023 The Royal Society of Chemistry.

The influence of the presence of short-chain ligands on the PQD surfaces was studied by Chen *et al.* (Fig. 17a). Chen *et al.*[169] successfully synthesized $CsPbI_3$ PQDs with excellent stability by partially replacing the OA/OAm ligands with octanoic/octylamine (C8) ligands. They further demonstrated that the short-chain ligands exhibited stronger adsorption on the PQD surface compared to the long-chain ligands, thereby inhibiting the defects formed due to ligand loss. Moreover, the PL intensity of the C8/C18-$CsPbI_3$ QDs can maintain ≈80% of its initial value for 180 days. In addition, they achieved a high J_{SC} of 16.98 mA cm^{-2} and a PCE of 11.87% in the $CsPbI_3$ PQD solar cells. The short-chain ligand substitution strategy may provide an avenue to alleviate adverse effects of insulated capping ligands on charge transport within PQD solid film. However, the authors emphasize that ligands that are too short (equal to or less than six carbon atoms) are not suitable for protecting PQD surfaces. In these cases, the photoactive structure is rapidly transformed into the orthorhombic yellow phase. A mixture of C8/C18 is indeed the optimal condition found according to a series of ligands evaluated. Recently, Shi *et al.*[170] reported the use of L-phenylalanine (L-PHE) in the *in situ* management of the surface ligand environment of high-quality $CsPbI_3$ QDs. This ligand is also not so easily lost from the $CsPbI_3$-QD surfaces compared with OA and OAm due to its higher adsorption energy. The optimal L-PHE-capped $CsPbI_3$ QDs display a significantly improved PLQY approaching 100%, longer free carrier lifetime, improved stability and fewer trap states (Fig. 17b). The increased dot-to-dot charge transfer in a film and passivating of defects boosted the optoelectronic performance. Therefore, the L-PHE capped $CsPbI_3$ QDs show versatility for applications in both photovoltaic devices and red LED devices, and a high PCE of 14.62% and an EQE of 10.21% are reported. Ligand exchanges are challenging because they may damage the PQD when exchanging ligands. However, short-chain ligands typically have low boiling points and special attention must be paid to temperature during hot-injection synthesis.[169]

Published on 27 de setembre 2023. Downloaded on 11/2/2026 22:48:11.

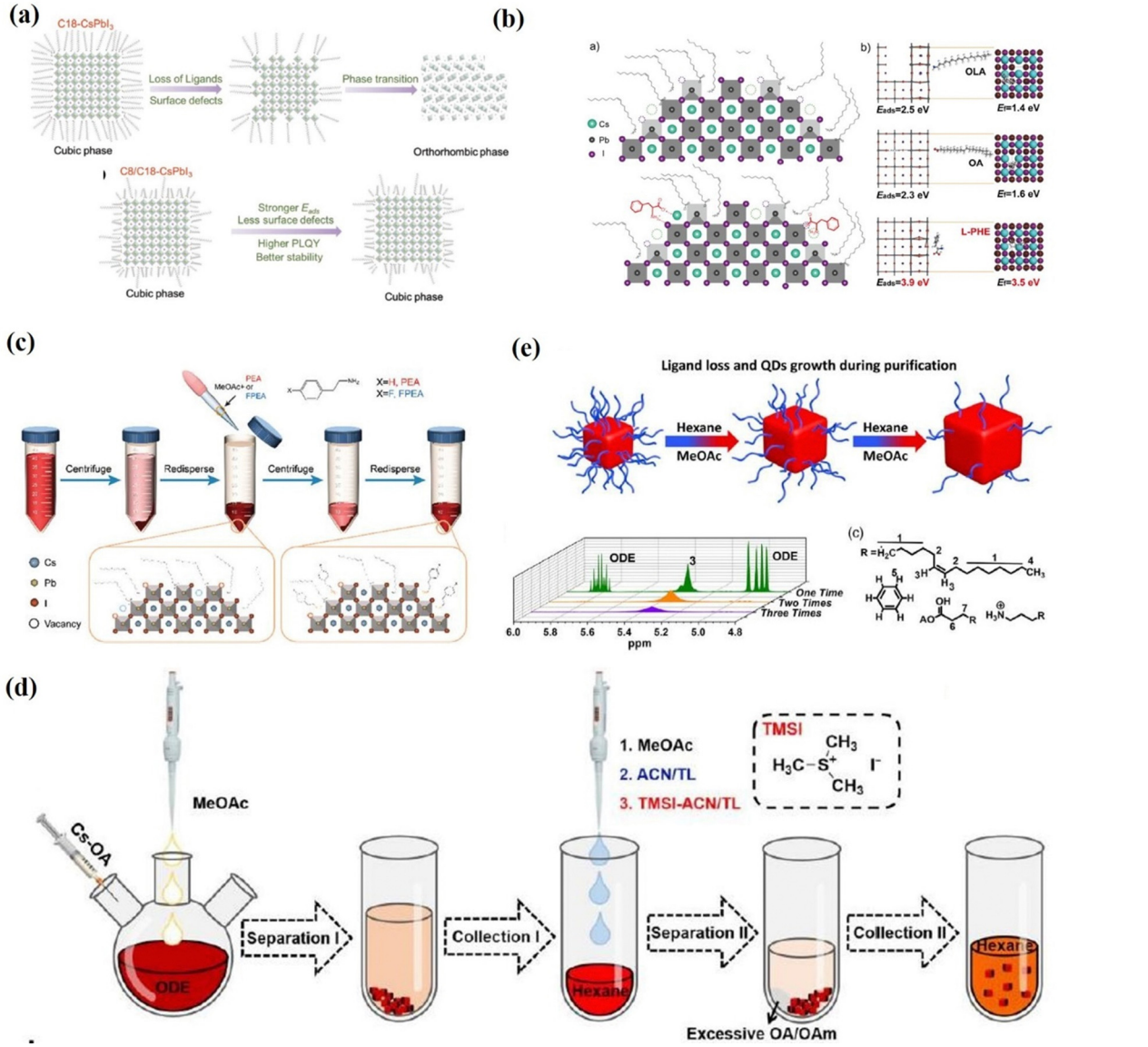

Fig. 17 (a) Schematic of the $CsPbI_3$ α-phase stabilization mechanism due to the presence of C8. Reproduced with permission from ref. 169. Copyright 2019, Wiley-VCH. (b) Schematic of the surface of the as-synthesized $CsPbI_3$ perovskite QDs with and without L-PHE passivation and the DFT calculated adsorption energy (*E*ads) of OA, OAm and L-PHE ligands on the optimized $CsPbI_3$ surfaces, and the corresponding formation energy of vacancy (E_f) on $CsPbI_3$ surfaces after the adsorption of different ligands. Reproduced with permission from ref. 170. Copyright 2020, Wiley-VCH. (c) A schematic diagram of the pseudo-solution-phase ligand exchange (p-SPLE) process. Reproduced with permission ref. 171. Copyright 2021, The Royal Society of Chemistry. (d) Schematic presentation of the purification processes of PQDs, in which the ligand riveting treatment was conducted after the ''Collection I'' process. Reproduced with permission ref. 172. Copyright 2022, The Royal Society of Chemistry. (e) A schematic illustration of QD changes during treatments and the full 1H NMR spectrum of the 1–3 times treatments of $CsPbBrI_2$ QDs in deuterated chloroform. Reproduced with permission from ref. 173. Copyright 2020, Wiley-VCH.

Besides the *in situ* substitution of ligands on the surface of $CsPbI_3$ QDs, ligand substitution during the washing of the QDs is also of critical importance. A pseudo solution ligand exchange was developed by Zhang *et al.*[171] to partly substitute the long insulating ligands of OA and OAm with PEA or 2-(4-fluorophenyl)ethyl ammonium (FPEA) as shown in Fig. 17c. The short and functional PEA and FPEA ligands could efficiently passivate the surface defects and suppress the non-radiative recombination, leading to an enhancement of PLQY (73.4% for the control QDs, 82.6% for PEA and 88.1% for FPEA-based $CsPbI_3$ QDs). Both PEA and FPEA treated $CsPbI_3$ QDs exhibited an improved PV performance, obtaining a champion PCE of 14.65%. Jia *et al.*[172] dissolved TMSI in a solvent mixture of acetonitrile (ACN) and toluene (TL) and used it as a counter-solvent for the second cleaning of the quantum dots as shown in Fig. 17d. Through robustly riveting TMSI ligands with an inverted triangular-pyramidal cationic structure into surface vacancies of PQDs, distortions of the $[PbI_6]^{4-}$ octahedral frameworks were suppressed by the consistent tensile strain imposed from the steric hindrance of the aprotic TMS^+. Consequently,

Published on 27 de setembre 2023. Downloaded on 11/2/2026 22:48:11.

the photophysical properties, crystallographic orientation and the energy landscape of PQD solids were significantly improved, leading to a PCE of up to 16.64% being realized in PQD solar cells, the highest efficiency among inorganic PQD solar cells.

In addition to controlling the length of the surface ligands, the management of the number of surface ligands is also very important. Liu *et al.*[173] precisely controlled and quantified the ligand amount relating to the $CsPbBrI_2$ PQDs based on a facile, hexane/MeOAc treatment, and further systematically studied the impact of the ligand amount on the final device performance. Without destroying the solubility, they precisely controlled the ligand amount around the PQDs at 1.01 wt% (Fig. 17e). The device fabricated from PQDs with lower ligand amounts exhibit better film quality, higher carrier mobility, and more efficient charge extraction than devices with higher ligand amounts. Therefore, they achieved a high J_{SC} of 14.22 mA cm^{-2} and a PCE as high as 12.2%. Although the annealing process reduced the interfaces between the PQDs by crystal fusion, this process is not suitable for all kinds of PQD solar cells, especially for $CsPbI_3$ and $FAPbI_3$, as the phase stability was attributed to the large contribution of the surface energy.[17,70]

Through a liquid-phase ligand engineering strategy, the mixed cesium and formamidinium lead triiodide QD ($Cs_{1-x}FA_xPbI_3$ QDs) solar cells also achieved high PCEs.[174–177] Hazarika *et al.*[175] reported a cation exchange post-treatment method to tune cations at the A-site in PQDs, which exhibited tunable PL emission within a range of 650–800 nm (Fig. 18a). The solar-cell performance with these alloyed QD inks showed an increased voltage approaching the Shockley–Queisser limit compared with the bulk perovskite devices. However, the occurrence of A-site cation exchange does not seem as easy as the halide anion exchange in the PQDs, and thus a driving force for A-site cation exchange of PQDs may be needed. Therefore, A-site cation exchange needs to be done at high temperatures and for long periods of time as shown in Fig. 18b. A feasible ligand-assisted cation exchange strategy of PQDs was demonstrated by Hao *et al.*[176] in which no heating was needed and high-quality $Cs_{1-x}FA_xPbI_3$ PQDs with good stability were obtained. The oleic acid-rich environment could promote A-site ion migration and diffusion in the $CsPbI_3$ and $FAPbI_3$ matrices (Fig. 18c). Encouragingly, the PQD solar cells device fabricated with $Cs_{0.5}FA_{0.5}PbI_3$ QDs delivered a certified efficiency of 16.6%, which is the highest certified PCE of PQD solar cells reported so far. Recently, Jia *et al.*[177] developed a feasible antisolvent-assisted *in situ* cation exchange of PQDs for finely regulating the stoichiometry of PQDs to tailor the optoelectronic properties and tolerance factors of PQDs (Fig. 18d). The light absorption spectra and tolerance factor of $Cs_{1-x}FA_xPbI_3$ QDs can be finely tuned by controlling the stoichiometries of FA^+ cations in the $Cs_{1-x}FA_xPbI_3$ QDs. As a consequence, the PQD solar cells yielded a PCE of up to 17.29%, the highest value among the reported homo structured PQD solar cells.

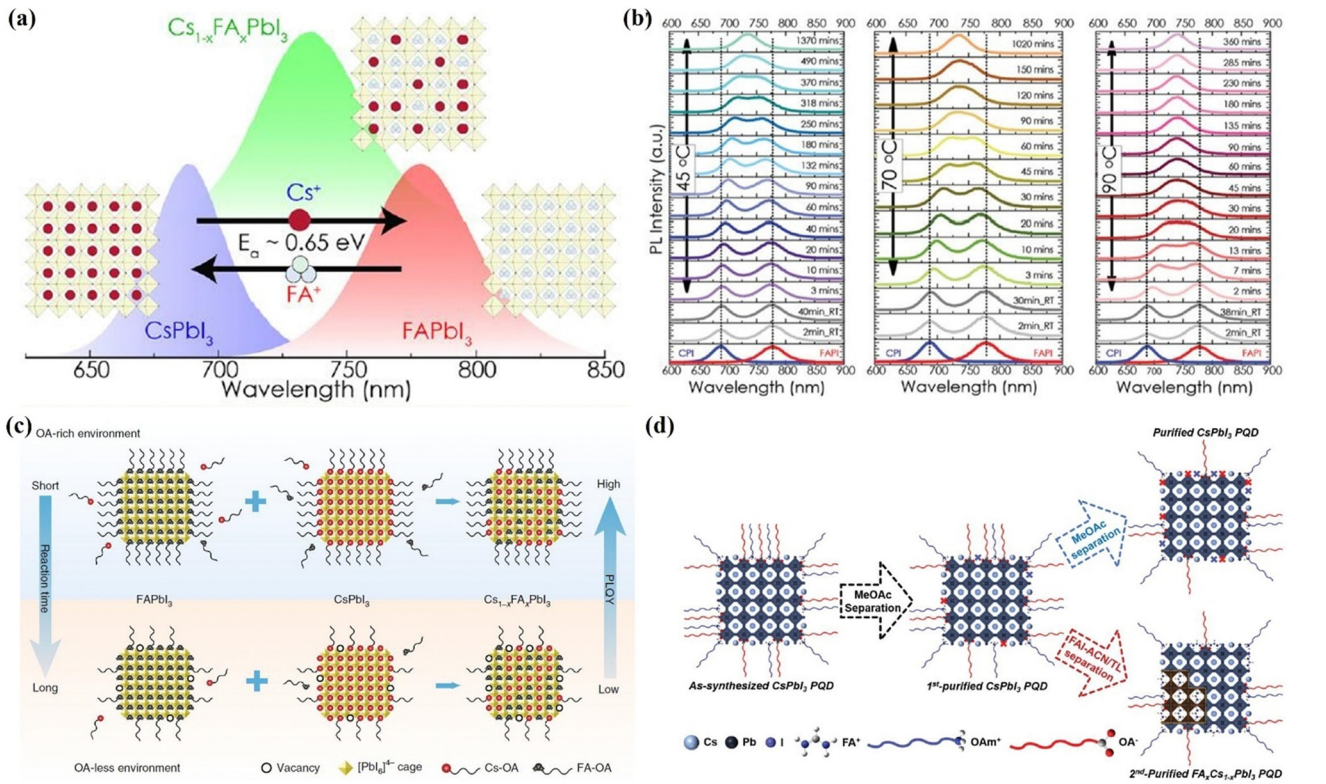

Fig. 18 (a) Illustration of the A-site cation exchange process and the corresponding PL spectra of PQDs. (b) Temperature-dependent kinetics of A-site cation exchange of PQDs. (a) and (b) Reprinted with permission from ref. 174. Copyright 2018 American Chemical Society. (c) Schematic diagram of the ligand-assisted A-site cation exchange of PQDs. Reprinted with permission from ref. 175. Copyright 2020 Nature Publishing Group. (d) Schematic illustration of the purification and post synthetic cation exchange of PQDs. Reprinted with permission from ref. 176. Copyright 2023 Wiley-VCH.

Published on 27 de setembre 2023. Downloaded on 11/2/2026 22:48:11.

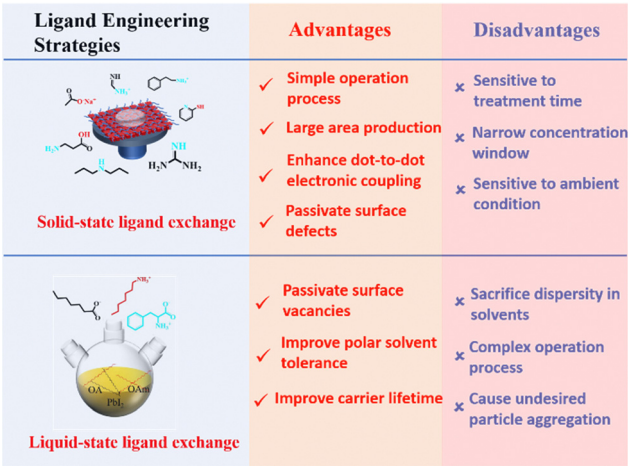

Fig. 19 A summary of the advantages and disadvantages of different ligand engineering strategies.

Hence, surface ligand regulation engineering provides an important way to improve the photovoltaic performance and stability of PQD solar cells. A summary of the advantages and disadvantages of different ligand engineering strategies is shown in Fig. 19. Table 1 summarizes the key photovoltaic parameters of PQD solar cells adopting various types of surface engineering. However, there is a paucity of fundamental studies on the detailed processes of ligand exchange in liquid and solid states. We should search for more new ligands to completely remove the long-chain ligands from the PQD surface while maintaining the high stability of PQD solid films.

4.2 Surface vacancy defect passivation

Charge recombination loss caused by the defect states in PQDs is one of the critical factors for the low efficiency of PQD solar cells.[29,59,61] Purification of the as-synthesized PQDs and deposition of PQD solid films assisted by anti-solvent also generated a number of surface vacancies, resulting in defect-assisted non-radiative recombination in the PQDs.[17,29,70] Therefore, to improve the performance of PQD solar cells, it is necessary to prepare PQD solutions and PQD films with a low vacancy defect density.

Early studies have shown that the halogen vacancy is the most abundant defect in PQDs and halide-rich surfaces favor desirable optical properties.[106,115] Therefore, Zhang *et al.*[178] used ZnI_2 as the dopant to synthesize Zn-doped $CsPbI_3$ (Zn:$CsPbI_3$) QDs with the halide-rich surface. The additional I^- in the reaction system can regulate the crystal growth and reduce the I vacancy defects of the as-prepared $CsPbI_3$ QDs, achieving higher PLQYs. Moreover, Zn:$CsPbI_3$ QDs prevent iodide ion loss during the purification and film fabrication processes (Fig. 20a), thereby decreasing the density of I vacancy defect states in the final PQD film and reducing the charge recombination loss in solar cells. As a result, a high PCE of 16.07% was obtained, which is among the best efficiencies for $CsPbI_3$ QD solar cells. Hydroiodic acid (HI) has also been reported to introduce $CsPbI_3$ to passivate I^- vacancies. The addition of HI enables the fabrication of $CsPbI_3$ QDs with a reduced defect density, enhanced crystallinity, higher phase purity, and near-unity PLQY (Fig. 20b). Therefore, the efficiency of $CsPbI_3$ QD solar cells was enhanced from 14.07% to 15.72% together with enhanced storage stability.[179] As mentioned in Section 3.1, a three-precursor synthesis approach has been developed to obtain surface halogen-rich PQDs. Qian *et al.*[180] synthesized high-quality $CsPbI_3$ QDs using this method and applied them as active layers in solar cells (Fig. 20c). They systematically adjusted the feed ratios in the synthesis of $CsPbI_3$ QDs using a ternary method and revealed the effects of Pb/Cs and Pb/I ratios on the synthetic yields and photovoltaic properties of the obtained PQDs. The need for excess lead precursors in the traditional binary precursor method was

Table 1 A summary of the photovoltaic performance of PQD solar cells based on ligand engineering

PQDs	Strategies	J_{SC} (mA cm^{-2})	V_{OC} (V)	FF (%)	PCE (%)	Ref.
Solid-state ligand exchange						
$CsPbI_3$	FAI–EtOAc ligand exchange	14.37	1.20	78.0	13.40	127
$CsPbI_3$	NaOAc–MeOAc ligand exchange	15.21	1.18	74.2	13.30	136
$CsPbI_3$	PEAI–MeOAc ligand exchange	15.30	1.23	74.8	14.10	137
$CsPbI_3$	Glycine–EtOAc ligand exchange	17.66	1.22	63.4	13.66	141
$CsPbI_3$	DPA–MeOAc ligand exchange	15.84	1.24	75.5	14.90	142
$CsPbI_3$	CsAc–EtOAc ligand exchange	14.96	1.25	75.6	14.10	143
$CsPbI_3$	GASCN–EtOAc ligand exchange	15.85	1.25	76.7	15.21	151
$CsPbI_3$	4-MP–EtOAc ligand exchange	14.32	1.25	79.0	14.25	157
$CsPbI_3$	Cl–PeOH ligand exchange	17.80	1.27	73.1	16.53	138
$CsPbI_3$	EDTA–EtOAc ligand exchange	17.51	1.23	71.0	15.25	158
$CsPbBr_3$	NaOAc–BuOAc ligand exchange	4.68	1.59	56.9	4.23	164
$CsPbBr_3$	GASCN–acetone ligand exchange	4.49	1.54	72.4	5.01	165
$CsPbBr_3$	BA–EtOAc ligand exchange	4.84	1.59	71.0	5.46	166
$CsPbBr_3$	GuaAc–MeOAc ligand exchange	5.93	1.59	74.7	7.04	135
Liquid-state ligand exchange						
$CsPbI_3$	OctAc/OctAm synthesis ligand	16.98	1.04	67.2	11.87	169
$CsPbI_3$	L-PHE synthesis ligand	15.23	1.23	78.0	14.62	170
$CsPbI_3$	FPEA + MeOAc ligand exchange	15.38	1.27	74.7	14.65	171
$CsPbI_3$	TMSI + ACN/TL ligand exchange	17.65	1.26	74.8	16.64	172

Published on 27 de setembre 2023. Downloaded on 11/2/2026 22:48:11.

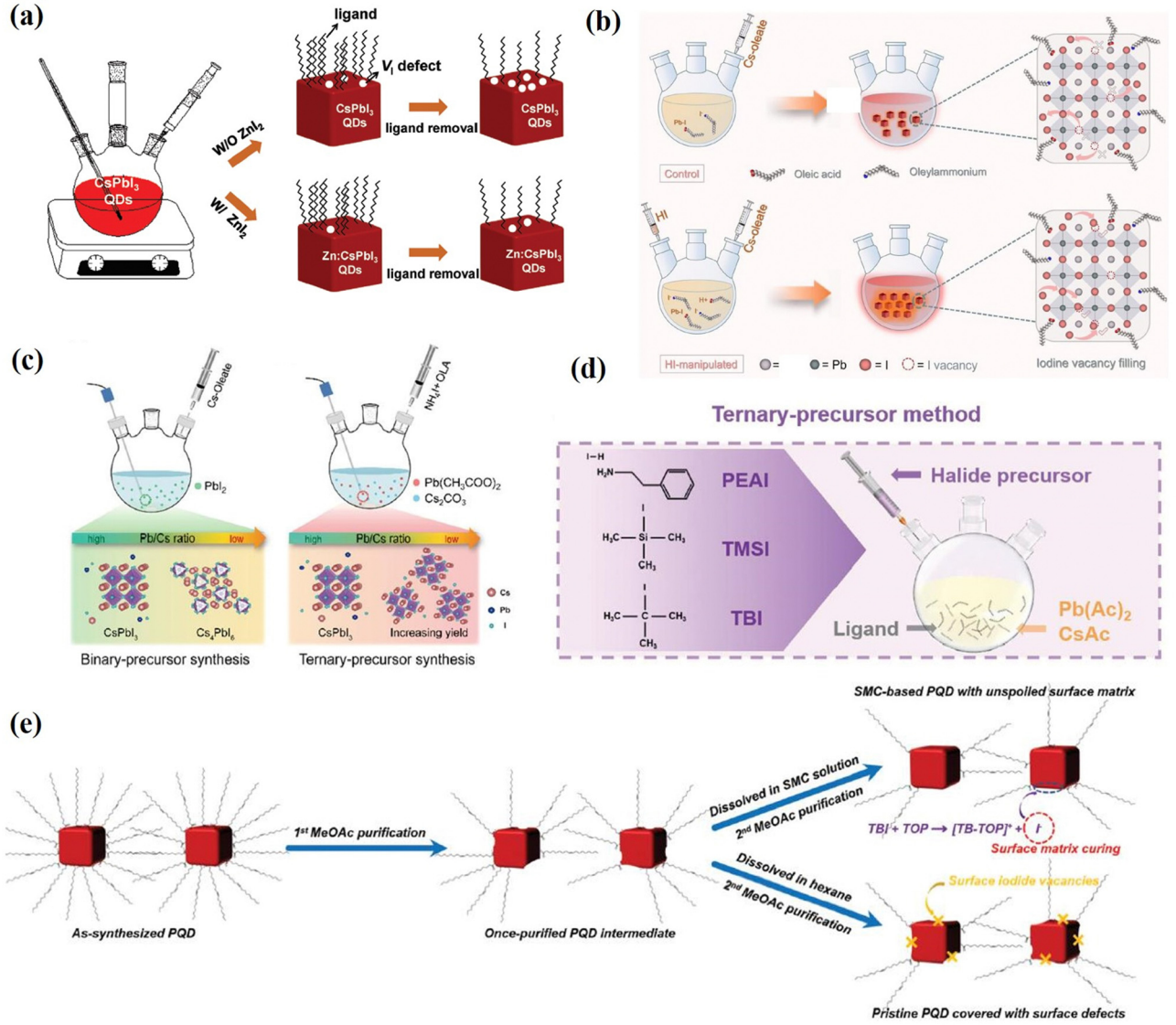

Fig. 20 (a) Schematic illustration of V_I defect state control by ZnI_2 during synthesis and ligand removal processes of $CsPbI_3$ QDs. Reproduced with permission from ref. 178. Copyright 2021, Wiley-VCH. (b) Schematic illustration of the $CsPbI_3$ QD synthesis process with and without HI manipulation. Reproduced with permission from ref. 179. Copyright 2023, Springer. (c) Illustration of synthesis based on a binary-precursor method and ternary-precursor method. Reproduced with permission from ref. 180. Copyright 2021, Wiley-VCH. (d) Schematic illustrations of ternary-precursor approaches for the synthesis of PQDs. Reproduced with permission from ref. 181. Copyright 2022, Wiley-VCH. (e) Schematic diagram of the SMC treatment of the PQDs with TBI-TOP. Reproduced with permission from ref. 182. Copyright 2021, The Royal Society of Chemistry.

found to be greatly alleviated in the ternary precursor protocol. A low ratio of Pb/Cs = 1 was adequate to maximize the utilization of cation precursors. Furthermore, the obtained $CsPbI_3$ QDs were applied to fabricate QD solar cells, showing a PCE of 14.24%, which is close to the reported state-of-the-art $CsPbI_3$ QD photovoltaic devices. In addition, a ternary-precursor approach is reported by Chen *et al.*[181] for the synthesis of PQDs in which the Cs, Pb, and I sources are derived from CsAc, $Pb(Ac)_2$ and trimethylsilyl iodide (TMSI) (Fig. 20d). The iodine-rich PQD was synthesized using the ternary-precursor method with the stripping effect of the nucleophilic TOP, which could substantially diminish nonradiative recombination and thus improve the optoelectronic properties of PQDs. Consequently, the PQD solar cell fabricated using the TMSI·TOP-based PQDs yielded a PCE of up to 16.25%, among the highest efficiencies of inorganic PQD solar cells.

Recently, a ''surface matrix curing'' (SMC) strategy was introduced by Jia *et al.*[182] They used a unimolecular nucleophilic substitution (S_N1) reaction of *tert*-butyl iodide (TBI) and the nucleophile trioctylphosphine (TOP), which can introduce sufficient iodide ions to fill the iodide vacancies of the PQD surface matrix (Fig. 20e). With this SMC strategy, the optoelectronic properties of the PQDs are significantly improved, and the non-radiative recombination caused by iodide vacancies is

Published on 27 de setembre 2023. Downloaded on 11/2/2026 22:48:11.

greatly reduced. As a result, the obtained SMC-based $CsPbI_3$ QDs are applied to fabricate QD solar cells yielding a high PCE of 16.21% (stabilized power output efficiency of 15.45%).

In summary, to obtain high-performance PQD solar cells, high quality PQD solutions and high quality PQD films are equally important. However, most of the current research is focused on how to prepare high quality films, and optimization of PQD solutions is relatively rare. Therefore, optimization of PQD solutions should be taken into account. In addition, a single surface treatment method cannot achieve optimal device performance. Combining with multiple treatment strategies, such as simultaneous regulation of ligand exchange and solvent optimization, may bring the device performance to a higher level.

Conclusions

This review provides an in-depth discussion on the surface engineering in $CsPbX_3$ PQDs and its influence on solar cell performance. We systematically analyze the surface chemistry of all inorganic PQDs, including the formation of surface vacancy defects and the surface ligand modification of PQDs. We summarize the corresponding surface defect passivation strategy for systematically improving the performance of PQD solar cells. The PCE trends of Cs-based PQD solar cells are summarized in Fig. 21. Despite significant progress in understanding the surface chemistry and the development of passivation strategies, there are still some important issues pertaining to further improve the stability and efficiency of the devices, which need to be fully addressed toward commercial applications in the future, as shown in Fig. 22.

(1) It is well known that the halide vacancies on the surface are the non-radiative recombination centers in PQDs. Due to the existence of surface defects, the incomplete surface is easily damaged by anti-solvent during the deposition of PQD solid films. Therefore, more attention should be paid to the passivation of PQD surface defects to minimize non-radiative recombination. However, most of the current studies are focused on the post-treatment of PQD films, while few studies are focused on defect passivation in the PQD solution. Therefore, further investigation should be centered on defect passivation in the PQD solution, which may reduce the defect density of PQD solid films, and the end result is better device performance. We can design it in the following two ways: ① *in situ* ligand exchange. Ligands such as DDBA,[78,79,82–86] IDA,[66] and TOP[96] proved to be effective in enhancing the optical properties of $CsPbX_3$ QDs. ② Passivation of QDs in the purification process. Addition of short-chain ligands to solvents or anti-solvents to treat PQDs.

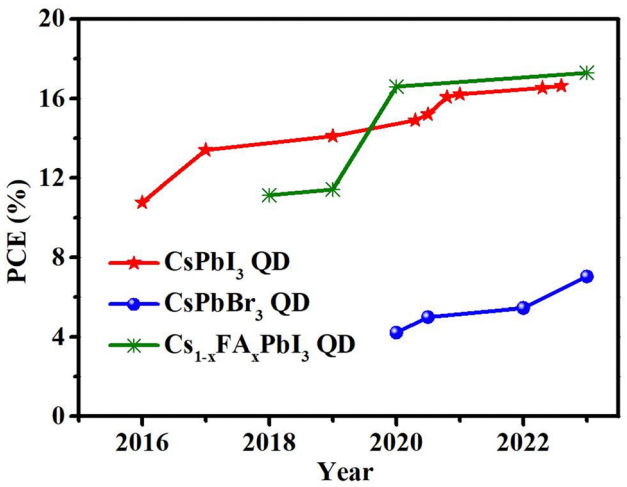

Fig. 21 The PCE evolution of PQD solar cells.

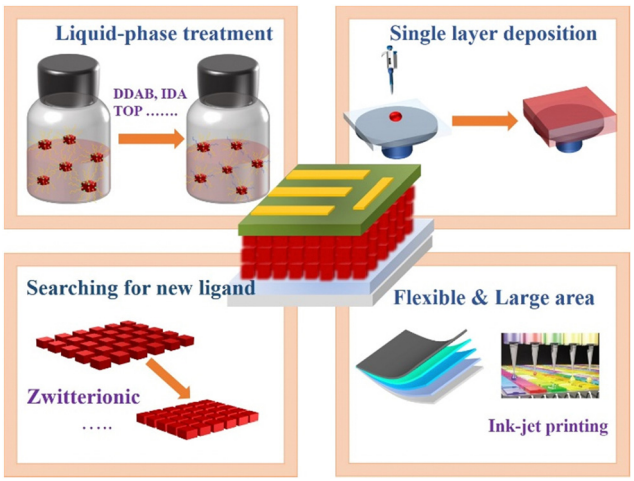

Fig. 22 Possible challenges and opportunities of PQD solar cells toward future development.

(2) Although OA/OAm ligand pairs have been adopted to synthesize PQDs in the majority of studies regarding PQD solar cells, they are highly dynamic and imprison the charges, resulting in poor device performance. Therefore, it is important to find a balance between surface passivation and dot-to-dot charge transport. Other short ligands with stronger interactions with PQDs should be explored. For example, the zwitterionic ligand[92–94] can tightly bound with the PQDs *via* the chelate effect, while the co-occurrences of cationic and anionic groups can prevent the external neutralization surroundings of PQDs, and thus enhance the structural durability of PQD films. Therefore, zwitterionic ligands should be further explored for application in solar cells.

(3) The film fabrication procedure of current PQD solar cells is mostly based on a layer-by-layer method. However, the layer-by-layer deposition method is complex and usually requires at least 3 to 5 layers of PQDs to achieve the desired film thickness. In addition, layer-by-layer deposition of PQD solid films make PQD solar cell devices have more interface than bulk devices, which induces undesired interfacial recombination. Therefore, further research should focus on developing a method to achieve the desired thickness through a single film deposition procedure. We suggest two methods: ① finding different anti-solvents (2-pentanol, acetonitrile, ethers *etc.*) to purify PQDs so that they remove as much of the surface ligand as possible

Published on 27 de setembre 2023. Downloaded on 11/2/2026 22:48:11.

without introducing defects. ② Searching for suitable solvents (chlorobenzene, chloroform, *etc.*) capable of dispersing PQDs in high concentrations to achieve sufficient thickness for monolayer deposition.

(4) Unlike polycrystalline thin film perovskites, a PQD film can be directly formed by simply depositing the colloidal QD inks without a further high temperature annealing procedure. It makes PQD promising in the field of large-area production on both rigid and flexible substrates to meet sustainable energy supply requirements. However, under the conventional synthesis route, PQDs need to undergo anti-solvent purification and repeated centrifugation to obtain colloidal solutions that are suitable for the deposition of PQD solid films, but the yield of PQDs is relatively low, which is not conducive to the realization of large-scale production. Therefore, the controlled synthesis of large-scale high-quality QD solutions is also a challenge. In addition, it is necessary to explore viable fabrication methods such as inkjet printing, spray-coating and Reel-to-Reel printing to fully utilize low-cost, solution-processable PQDs to deposit uniform, dense films.

In conclusion, despite the challenges in passivating surface defects of PQDs, its excellent and unique properties do not obscure its potential as a promising photovoltaic material. The key is to determine how to exploit these properties to obtain PQDs with ideal surfaces through synthetic chemistry, defect physics, spectral physics, *etc.* We predict that PQDs will receive increasing attention and become an emerging star in the field of photovoltaic research in the near future.

Conflicts of interest

There are no conflicts to declare.

Acknowledgements

This work was supported by the National Key Research and Development Program of China (2022YFB4200500), the Anhui Provincial Natural Science Foundation (2308085ME137, 2108085ME147), and the National Natural Science Foundation of Hefei City (2022024).

Notes and references

1 R. Rossetti, S. Nakahara and L. E. Brus, Quantum Size Effects in the Redox Potentials, Resonance Raman Spectra, and Electronic Spectra of CdS Crystallites in Aqueous Solution, *J. Chem. Phys.*, 1983, **79**, 1086–1088.

2 L. E. Brus, Electron-electron and Electron-hole Interactions in Small Semiconductor Crystallites: The Size Dependence of the Lowest Excited Electronic State, *J. Chem. Phys.*, 1984, **80**, 4403–4409.

3 L. E. Brus, Electronic Wave Functions in Semiconductor Clusters: Experiment and Theory, *J. Phys. Chem.*, 1986, **90**, 2555–2560.

4 J. J. Storhoff, A. A. Lazarides, R. C. Mucic, C. A. Mirkin, R. L. Letsinger and G. C. Schatz, What Controls the Optical Properties of DNA-Linked Gold Nanoparticle Assemblies?, *J. Am. Chem. Soc.*, 2000, **122**, 4640–4650.

5 C. P. Byers, H. Zhang, D. F. Swearer, M. Yorulmaz, B. S. Hoener, D. Huang, A. Hoggard, W.-S. Chang, P. Mulvaney, E. Ringe, N. J. Halas, P. Nordlander, S. Link and C. F. Landes, From Tunable Core-Shell Nanoparticles to Plasmonic Drawbridges: Active Control of Nanoparticle Optical Properties, *Sci. Adv.*, 2015, **1**, e1500988.

6 G. H. Carey, A. L. Abdelhady, Z. Ning, S. M. Thon, O. M. Bakr and E. H. Sargent, Colloidal Quantum Dot Solar Cells, *Chem. Rev.*, 2015, **115**, 12732–12763.

7 M. Yuan, M. Liu and E. H. Sargent, Colloidal Quantum Dot Solids for Solution-Processed Solar Cells, *Nat. Energy*, 2016, **1**, 16016.

8 G. Konstantatos, I. Howard, A. Fischer, S. Hoogland, J. Clifford, E. Klem, L. Levina and E. H. Sargent, Ultrasensitive Solution-Cast Quantum Dot Photodetectors, *Nature*, 2006, **442**, 180–183.

9 V. I. Klimova, A. Mikhailovsky, S. Xu, A. Malko, J. A. Hollingsworth, C. A. Leatherdale, H.-J. Eisler and M. G. Bawendi, Optical Gain and Stimulated Emission in Nanocrystal Quantum Dots, *Science*, 2000, **290**, 314–317.

10 X. Dai, Z. Zhang, Y. Jin, Y. Niu, H. Cao, X. Liang, L. Chen, J. Wang and X. Peng, Solution-Processed, High-Performance Light-Emitting Diodes Based on Quantum Dots, *Nature*, 2014, **515**, 96–99.

11 Y. Won, O. Cho, T. Kim, D. Chung, T. Kim, H. Chung, H. Jang, J. Lee, D. Kim and E. Jang, Highly Efficient and Stable InP/ZnSe/ZnS Quantum Dot Light-Emitting Diodes, *Nature*, 2019, **575**, 634–638.

12 M. V. Kovalenko, L. Manna, A. Cabot, Z. Hen, D. V. Talapin, C. R. Kagan, V. I. Klimov, A. L. Rogach, P. Reiss, D. J. Milliron, P. G.-Sionnnest, G. Konstantatos, W. J. Park, T. Hyeon, B. A. Korgel, C. B. Murray and W. Heiss, Prospects of Nanoscience with Nanocrystals, *ACS Nano*, 2015, **9**, 1012–1057.

13 M. C. Beard, J. M. Luther, O. E. Semonin and A. J. Nozik, Third Generation Photovoltaics based on Multiple Exciton Generation in Quantum Confined Semiconductors, *Acc. Chem. Res.*, 2013, **46**, 1252–1260.

14 M. Siguan, D. Koch, A. D. Taylor, Q. Sun, V. Lami, P. Oppenheimer, F. Paulus and Y. Vaynzof, Efficient and Stable PbS Quantum Dot Solar Cells by Triple-Cation Perovskite Passivation, *ACS Nano*, 2020, **14**, 384–393.

15 S. Chen, Y. J. Wang, Q. Liu, G. Shi, Z. Liu, K. Lu, L. Han, X. Ling, H. Zhang, S. Cheng and W. Ma, Broadband Enhancement of PbS Quantum Dot Solar Cells by the Synergistic Effect of Plasmonic Gold Nanobipyramids and Nanospheres, *Adv. Energy Mater.*, 2018, **8**, 1701194.

16 B. Sun, A. Johnston, C. Xu, M. Wei, Z. Huang, Z. Jiang, H. Zhou, Y. Gao, Y. Dong, O. Ouellette, X. Zheng, J. Liu, M.-J. Choi, Y. Gao, S.-W. Baek, F. Laquai, O. M. Bakr, D. Ban, O. Voznyy, F. P. G. de Arquer and E. H. Sargent, Monolayer

Published on 27 de setembre 2023. Downloaded on 11/2/2026 22:48:11.

Perovskite Bridges Enable Strong Quantum Dot Coupling for Efficient Solar Cells, *Joule*, 2020, **4**, 1542–1556.

17 A. Swarnkar, A. R. Marshall, E. M. Sanehira, B. D. Chernomordik, D. T. Moore, J. A. Christians, T. Chakrabarti and J. M. Luther, Quantum Dot–Induced Phase Stabilization of α-$CsPbI_3$ Perovskite for High-Efficiency Photovoltaics, *Science*, 2016, **354**, 92–95.

18 M. Hao, Y. Bai, S. Zeiske, L. Ren, J. Liu, Y. Yuan, N. Zarrabi, N. Cheng, M. Ghasemi, P. Chen, M. Lyu, D. He, J. Yun, Y. Du, Y. Wang, S. Ding, A. Armin, P. Meredith, G. Liu, H. Cheng and L. Wang, Ligand-Assisted Cation-Exchange Engineering for High-Efficiency Colloidal $Cs_{1-x}FA_xPbI_3$ Quantum Dot Solar Cells with Reduced Phase Segregation, *Nat. Energy*, 2020, **5**, 79–88.

19 J. Song, J. Li, X. Li, L. Xu, Y. Dong and H. Zeng, Quantum Dot Light-Emitting Diodes Based on Inorganic Perovskite Cesium Lead Halides ($CsPbX_3$), *Adv. Mater.*, 2015, **27**, 7162.

20 A. Pan, Y. Zhou, C. Zhao, C. Shi, Y. Wu, Y. Zhang, Y. Liu and L. He, Luminescent and Ultrastable Perovskite-Acrylate Based Elastomers with Excellent Stretchability and Self-healing Capability for Flexible Backlight Display, *Chem. Eng. J.*, 2022, **433**, 133590.

21 L. Protesescu, S. Yakunin, M. I. Bodnarchuk, F. Krieg, R. Caputo, C. H. Hendon, R. Yang, A. Walsh and M. V. Kovalenko, Nanocrystals of Cesium Lead Halide Perovskites ($CsPbX_3$, X = Cl, Br, and I): Novel Optoelectronic Materials Showing Bright Emission with Wide Color Gamut, *Nano Lett.*, 2015, **15**, 3692–3696.

22 J. J. Yoo, G. Seo, M. R. Chua, T. Park, Y. Lu, F. Rotermund, Y. Kim, C. Moon, N. Jeon, J. Baena, V. Bulović, S. Shin, M. G. Bawendi and J. Seo, Efficient Perovskite Solar Cells via Improved Carrier Management, *Nature*, 2021, **590**, 587–593.

23 I. Moreels, Y. Justo, B. De Geyter, K. Haustraete, J. C. Martins and Z. Hens, Size-Tunable, Bright, and Stable PbS Quantum Dots: A Surface Chemistry Study, *ACS Nano*, 2011, **5**, 2004–2012.

24 D. J. Milliron, The Surface Plays a Core Role, *Nat. Mater.*, 2014, **13**, 772–773.

25 A. H. Ip, S. M. Thon, S. Hoogland, O. Voznyy, D. Zhitomirsky, R. Debnath, L. Levina, L. R. Rollny, G. H. Carey, A. Fischer, K. W. Kemp, I. J. Kramer, Z. Ning, A. J. Labelle, K. Chou, A. Amassian and E. H. Sargent, Hybrid Passivated Colloidal Quantum Dot Solids, *Nat. Nanotechnol.*, 2012, **7**, 577–582.

26 M. Kazes, T. Udayabhaskararao, S. Dey and D. Oron, Effect of Surface Ligands in Perovskite Nanocrystals: Extending in and Reaching out, *Acc. Chem. Res.*, 2021, **54**, 1409–1418.

27 M. A. Boles, D. Ling, T. Hyeon and D. V. Talapin, The Surface Science of Nanocrystals, *Nat. Mater.*, 2016, **15**, 141–153.

28 A. Dey, J. Ye, A. De, E. Debroye, S. K. Ha, E. Bladt, A. S. Kshirsagar, Z. Wang, J. Yin, Y. Wang, L. Quan, F. Yan, M. Gao, X. Li, J. Shamsi, T. Debnath, M. Cao, M. A. Scheel, S. Kumar, J. A. Steele, M. Gerhard, L. Chouhan, K. Xu, X. Wu, Y. Li, Y. Zhang, A. Dutta, C. Han, I. Vincon, A. L. Rogach, A. Nag, A. Samanta, B. A. Korgel, C. Shih, D. R. Gamelin, D. Son, H. Zeng, H. Zhong, H. Sun, H. Demir, I. G. Scheblykin, I. Seró, J. K. Stolarczyk, J. Z. Zhang, J. Feldmann, J. Hofkens, J. M. Luther, J. Prieto, L. Li, L. Manna, M. I. Bodnarchuk, M. V. Kovalenko, M. B. J. Roeffaers, N. Pradhan, O. F. Mohammed, O. M. Bakr, P. Yang, P. Buschbaum, P. V. Kamat, Q. Bao, Q. Zhang, R. Krahne, R. E. Galian, S. D. Stranks, S. Bals, V. Biju, W. A. Tisdale, Y. Yan, R. L. Z. Hoye and L. Polavarapu, State of the Art and Prospects for Halide Perovskite Nanocrystals, *ACS Nano*, 2021, **15**, 10775–10981.

29 S. Seth, T. Ahmed, A. De and A. Samanta, Tackling the Defects, Stability, and Photoluminescence of $CsPbX_3$ Perovskite Nanocrystals, *ACS Energy Lett.*, 2019, **4**, 1610–1618.

30 Y. Chen, S. R. Smock, A. H. Flintgruber, F. A. Perras, R. L. Brutchey and A. J. Rossini, Surface Termination of $CsPbBr_3$ Perovskite Quantum Dots Determined by Solid-State NMR Spectroscopy, *J. Am. Chem. Soc.*, 2020, **142**, 6117–6127.

31 K. Hills-Kimball, H. Yang, T. Cai, J. Wang and O. Chen, Recent Advances in Ligand Design and Engineering in Lead Halide Perovskite Nanocrystals, *Adv. Sci.*, 2021, **8**, 2100214.

32 J. Yuan, A. Hazarika, Q. Zhao, X. Ling, T. Moot, W. Ma and J. M. Luther, Transmission Capacity Expansion is Needed to Decarbonize the Electricity Sector Efficiently, *Joule*, 2020, **4**, 1–3.

33 A. O. El-Ballouli, O. M. Bakr and O. F. Mohammed, Compositional, Processing, and Interfacial Engineering of Nanocrystal-and Quantum-Dot-Based Perovskite Solar Cells, *Chem. Mater.*, 2019, **31**, 6387–6411.

34 J. Chen, D. Jia, E. M. J. Johansson, A. Hagfeldt and X. Zhang, Emerging Perovskite Quantum Dot Solar Cells: Feasible Approaches to Boost Performance, *Energy Environ. Sci.*, 2021, **14**, 224–261.

35 W. Sun, R. Yun, Y. Liu, X. Zhang, M. Yuan, L. Zhang and X. Li, Ligands in Lead Halide Perovskite Nanocrystals: From Synthesis to Optoelectronic Applications, *Small*, 2022, **19**, 2205950.

36 G. Rose, De perowskite, fossili novo, *De Novis Quibusdam Fossilibus Quae in Montibus Uraliis Inveniuntur*, Verlagsort, Berlin, Germany, 1839.

37 D. B. Straus, S. Guo, A. M. Abeykoon and R. J. Cava, Understanding the Instability of the Halide Perovskite $CsPbI_3$ through Temperature-Dependent Structural Analysis, *Adv. Mater.*, 2020, **32**, 2001069.

38 J. Yuan, D. Zhou, C. Zhuang, Y. Zhou, C. Zhang, L. Wang, M. Xiao and X. Wang, Single-Photon Emission from Single Microplate $MAPbI_3$ Nanocrystals with Ultranarrow Photoluminescence Linewidths and Exciton Fine Structures, *Adv. Opt. Mater.*, 2022, **10**, 2200606.

39 J. Park, J. Kim, H.-S. Yun, M. Paik, E. Noh, H. Mun, M. G. Kim, T. J. Shin and S. Seok, Controlled growth of perovskite layers with volatile alkylammonium chlorides, *Nature*, 2023, **616**, 724–730.

40 X. Zhang, H. Huang, L. Jin, C. Wen, Q. Zhao, C. Zhao, J. Guo, C. Cheng, H. Wang, L. Zhang, Y. Li, Y. Maung,

Published on 27 de setembre 2023. Downloaded on 11/2/2026 22:48:11.

J. Yuan and W. Ma, Ligand-Assisted Coupling Manipulation for Efficient and Stable $FAPbI_3$ Colloidal Quantum Dot Solar Cells, *Angew. Chem., Int. Ed.*, 2023, **62**, e2022142.

41 B. Kshirsagar, N. Jaykhedkar, K. Jain, S. Kishor, V. Shah, L. M. Ramaniah and S. Tiwari, Green $CsSnX_3$ (X = Cl, Br, I)-Derived Quantum Dots for Photovoltaic Applications: First-Principles Investigations, *J. Phys. Chem. C*, 2021, **125**, 2592–2606.

42 X. Ling, J. Yuan and W. Ma, The Rise of Colloidal Lead Halide Perovskite Quantum Dot Solar Cells, *Acc. Mater. Res.*, 2022, **3**, 866–878.

43 P. Wang, C. Gong, G. Rao, K. Hu, X. Wang, C. Yan, L. Dai, C. Wu and J. Xiong, Recent Advances in Halide Perovskite Photodetectors Based on Different Dimensional Materials, *Adv. Opt. Mater.*, 2018, **6**, 1701302.

44 C. J. Bartel, C. Sutton, B. R. Goldsmith, R. Ouyang, C. B. Musgrave, L. M. Ghiringhelli and M. Scheffler, New Tolerance Factor to Predict the Stability of Perovskite Oxides and Halides, *Sci. Adv.*, 2019, **5**, eaav0693.

45 L. Liu, A. Najar, K. Wang, M. Du and S. Liu, Perovskite Quantum Dots in Solar Cells, *Adv. Sci.*, 2022, **9**, 2104577.

46 V. M. Goldschmidt, Die Gesetze der Krystallochemie, *Naturwissenschaften*, 1926, **14**, 477–485.

47 Y. Wei, Z. Cheng and J. Lin, An Overview on Enhancing the Stability of Lead Halide Perovskite Quantum Dots and Their Applications in Phosphor-Converted LEDs, *Chem. Soc. Rev.*, 2019, **48**, 310–350.

48 C. Li, X. Lu, W. Ding, L. Feng, Y. Gao and Z. Guo, Formability of ABX_3 (X = F, Cl, Br, I) Halide Perovskites, *Acta Crystallogr., Sect. B: Struct. Sci.*, 2008, **64**, 702–707.

49 Database of Ionic Radii, **https://abulafia.mt.ic.ac.uk/shannon/ptable.php**, accessed February 1, 2019.

50 R. J. Sutton, M. R. Filip, A. A. Haghighirad, N. Sakai, B. Wenger, F. Giustino and H. J. Snaith, Cubic or Orthorhombic? Revealing the Crystal Structure of Metastable Black-Phase $CsPbI_3$ by Theory and Experiment, *ACS Energy Lett.*, 2018, **3**, 1787–1795.

51 A. Dutta and N. Pradhan, Phase-Stable Red-Emitting $CsPbI_3$ Nanocrystals: Successes and Challenges, *ACS Energy Lett.*, 2019, **4**, 709–719.

52 R. E. Brandt, J. R. Poindexter, P. Gorai, R. C. Kurchin, R. L. Z. Hoye, L. Nienhaus, M. W. B. Wilson, J. A. Polizzotti, R. Sereika, R. Z. Altauskas, L. C. Lee, J. L. MacManus-Driscoll, M. Bawendi, V. Stevanović and T. Buonassisi, Searching for "Defect-Tolerant" Photovoltaic Materials: Combined Theoretical and Experimental Screening, *Chem. Mater.*, 2017, **29**, 4667–4674.

53 R. E. Brandt, V. Stevanović, D. S. Ginley and T. Buonassisi, Identifying Defect-Tolerant Semiconductors with High Minority-Carrier Lifetimes: Beyond Hybrid Lead Halide Perovskites, *MRS Commun.*, 2015, **5**, 265–275.

54 Q. A. Akkerman, G. Rainò, M. V. Kovalenko and L. Manna, Challenges and Opportunities for Colloidal Lead Halide Perovskite Nanocrystals, *Nat. Mater.*, 2018, **17**, 394–405.

55 A. Buin, P. Pietsch, J. Xu, O. Voznyy, A. H. Ip, R. Comin and E. H. Sargent, Materials Processing Routes to Trap-Free Halide Perovskites, *Nano Lett.*, 2014, **14**, 6281–6286.

56 T. Takagahara and K. Takeda, Theory of the Quantum Confinement Effect on Excitons in Quantum Dots of Indirect-Gap Materials, *Phys. Rev. B: Condens. Matter Mater. Phys.*, 1992, **46**, 15578.

57 R. Koole, E. Groeneveld, D. Vanmaekelbergh, A. Meijerink and C. D. M. Donegá, Size Effects on Semiconductor Nanoparticles, Nanoparticles-Workhorses of Nanoscience, ch. 2, 2005.

58 A. D. Yoffe, Low-Dimensional Systems: Quantum Size Effects and Electronic Properties of Semiconductor Microcrystallites (Zero-Dimensional Systems) and Some Quasi-Two-Dimensional Systems, *Adv. Phys.*, 1993, **42**, 173–262.

59 F. W. Eagle, N. Park, M. Cash and B. M. Cossairt, Surface Chemistry and Quantum Dot Luminescence: Shell Growth, Atomistic Modification, and Beyond, *ACS Energy Lett.*, 2021, **6**, 977–984.

60 S. Brinck and I. Infante, Surface Termination, Morphology, and Bright Photoluminescence of Cesium Lead Halide Perovskite Nanocrystals, *ACS Energy Lett.*, 2016, **1**, 1266–1272.

61 M. I. Bodnarchuk, S. C. Boehme, S. Brinck, C. Bernasconi, Y. Shynkarenko, F. Krieg, R. Widmer, B. Aeschlimann, D. Günther, M. V. Kovalenko and I. Infante, Rationalizing and Controlling the Surface Structure and Electronic Passivation of Cesium Lead Halide Nanocrystals, *ACS Energy Lett.*, 2019, **4**, 63–74.

62 G. Almeida, I. Infante and L. Manna, Resurfacing halide perovskite nanocrystals, *Science*, 2019, **364**, 833–834.

63 D. Chen, P. K. Ko, C. H. Angus, B. Zou, P. Geng, L. Guo and J. E. Halpert, Amino Acid-Passivated Pure Red $CsPbI_3$ Quantum Dot LEDs, *ACS Energy Lett.*, 2023, **8**, 410–416.

64 R. Han, Q. Zhao, A. Hazarika, J. Li, H. Cai, J. Ni and J. Zhang, Ionic Liquids Modulating $CsPbI_3$ Colloidal Quantum Dots Enable Improved Mobility for High-Performance Solar Cells, *ACS Appl. Mater. Interfaces*, 2022, **14**, 4061–4070.

65 A. Pan, B. He, X. Fan, Z. Liu, J. J. Urban, A. P. Alivisatos, L. He and Y. Liu, Insight into the Ligand-Mediated Synthesis of Colloidal $CsPbBr_3$ Perovskite Nanocrystals: The Role of Organic Acid, Base, and Cesium Precursors, *ACS Nano*, 2016, **10**, 7943–7954.

66 J. Pan, Y. Shang, J. Yin, M. D. Bastiani, W. Peng, I. Dursun, L. Sinatra, A. M. El-Zohry, M. N. Hedhili, A. Emwas, O. F. Mohammed, Z. Ning and O. M. Bakr, Bidentate Ligand-Passivated $CsPbI_3$ Perovskite Nanocrystals for Stable Near-Unity Photoluminescence Quantum Yield and Efficient Red Light-Emitting Diodes, *J. Am. Chem. Soc.*, 2018, **140**, 562–565.

67 J. D. Roo, M. Ibáñez, P. Geiregat, G. Nedelcu, W. Walravens, J. Maes, J. C. Martins, I. V. Driessche, M. V. Kovalenko and Z. Hens, Highly Dynamic Ligand Binding and Light Absorption Coefficient of Cesium Lead Bromide Perovskite Nanocrystals, *ACS Nano*, 2016, **10**, 2071–2081.

68 H. Huang, X. Zhang, C. Zhao and J. Yuan, Efficient and stable hybrid conjugated polymer/perovskite quantum dot solar cells, *Mater. Chem. Front.*, 2023, **7**, 1423–1430.

Published on 27 de setembre 2023. Downloaded on 11/2/2026 22:48:11.

69 S. Ding, M. Hao, C. Fu, T. Lin, A. Baktash, P. Chen, D. He, C. Zhang, W. Chen, A. K. Whittaker, Y. Bai and L. Wang, In Situ Bonding Regulation of Surface Ligands for Efficient and Stable $FAPbI_3$ Quantum Dot Solar Cells, *Adv. Sci.*, 2022, **9**, 2204476.

70 J. Xue, J.-W. Lee, Z. Dai, R. Wang, S. Nuryyeva, M. E. Liao, S.-Y. Chang, L. Meng, D. Meng, P. Sun, O. Lin, M. S. Goorsky and Y. Yang, Surface Ligand Management for Stable $FAPbI_3$ Perovskite Quantum Dot Solar Cells, *Joule*, 2018, **2**, 1866–1878.

71 S. Ding, M. Hao, T. Lin, Y. Bai and L. Wang, Ligand Engineering of Perovskite Quantum Dots for Efficient and Stable Solar Cells, *J. Energy Chem.*, 2022, **69**, 626–648.

72 C. Bi, Z. Yao, X. Sun, X. Wei, J. Wang and J. Tian, Perovskite Quantum Dots with Ultralow Trap Density by Acid Etching-Driven Ligand Exchange for High Luminance and Stable Pure-Blue Light-Emitting Diodes, *Adv. Mater.*, 2021, **33**, 2006722.

73 D. P. Nenon, K. Pressler, J. Kang, B. A. Koscher, J. H. Olshansky, W. T. Osowiecki, M. A. Koc, L. W. Wang and A. P. Alivisatos, Design Principles for Trap-Free $CsPbX_3$ Nanocrystals: Enumerating and Eliminating Surface Halide Vacancies with Softer Lewis Bases, *J. Am. Chem. Soc.*, 2018, **140**, 17760–17772.

74 V. K. Ravi, P. K. Santra, N. Joshi, J. Chugh, S. K. Singh, H. Rensmo, P. Ghosh and A. Nag, Origin of the Substitution Mechanism for the Binding of Organic Ligands on the Surface of $CsPbBr_3$ Perovskite Nanocubes, *J. Phys. Chem. Lett.*, 2017, **8**, 4988–4994.

75 M. L. H. Green, The Formal Classification of Covalent Compounds of The Elements, *Organomet. Chem.*, 1995, **500**, 127–148.

76 N. K. Noel, A. Abate, S. D. Stranks, E. S. Parrott, V. M. Burlakov, A. Goriely and H. J. Snaith, Enhanced Photoluminescence and Solar Cell Performance via Lewis Base Passivation of Organic-Inorganic Lead Halide Perovskites, *ACS Nano*, 2014, **8**, 9815–9821.

77 S. M. Park, A. Abtahi, A. M. Boehm and K. R. Graham, Surface Ligands for Methylammonium Lead Iodide Films: Surface Coverage, Energetics, and Photovoltaic Performance, *ACS Energy Lett.*, 2020, **5**, 799–806.

78 J. Pan, S. P. Sarmah, B. Murali, I. Dursun, W. Peng, M. R. Parida, J. Liu, L. Sinatra, N. Alyami, C. Zhao, E. Alarousu, T. K. Ng, B. S. Ooi, O. M. Bakr and O. F. Mohammed, Air-Stable Surface-Passivated Perovskite Quantum Dots for Ultra-Robust, Single- and Two-Photon-Induced Amplified Spontaneous Emission, *J. Phys. Chem. Lett.*, 2015, **6**, 5027–5033.

79 J. Pan, L. N. Quan, Y. Zhao, W. Peng, B. Murali, S. P. Sarmah, M. Yuan, L. Sinatra, N. M. Alyami, J. Liu, E. Yassitepe, Z. Yang, O. Voznyy, R. Comin, M. N. Hedhili, O. F. Mohammed, Z. H. Lu, D. H. Kim, E. H. Sargent and O. M. Bakr, Highly Efficient Perovskite-Quantum-Dot Light-Emitting Diodes by Surface Engineering, *Adv. Mater.*, 2016, **28**, 8718.

80 M. Wang, Z. Lei, C. Du, Y. Wen, B. Shan, K. Cao and R. Chen, Stabilization of $CsPbBr_3$ Nanocrystals via Defect Passivation and Alumina Encapsulation for High-Power Light-Emitting Diodes, *ACS Appl. Nano Mater.*, 2023, **6**, 6480–6487.

81 H. Zhu, Y. Pan, C. Peng, H. Lian and J. Lin, 4-Bromo-Butyric Acid-Assisted in Situ Passivation Strategy for Super Stable All-Inorganic Halide Perovskite $CsPbX_3$ Quantum Dots in Polar Media, *Angew. Chem., Int. Ed.*, 2022, **61**, e202116702.

82 Y. Huang, W. Luan, M. Liu and L. Turyanska, DDAB-Assisted Synthesis of Iodine-Rich $CsPbI_3$ Perovskite Nanocrystals with Improved Stability in Multiple Environments, *J. Mater. Chem. C*, 2020, **8**, 2381–2387.

83 H. Wu, Y. Zhang, M. Lu, X. Zhang, C. Sun, T. Zhang, V. L. Colvin and W. Y. William, Surface Ligand Modification of Cesium Lead Bromide Nanocrystals for Improved Light-Emitting Performance, *Nanoscale*, 2018, **10**, 4173–4178.

84 J. Park, A. Lee, J. C. Yu, Y. Nam, Y. Choi, J. Park and M. H. Song, Surface Ligand Engineering for Efficient Perovskite Nanocrystal-Based Light-Emitting Diodes, *ACS Appl. Mater. Interfaces*, 2019, **11**, 8428–8435.

85 A. F. Gualdrón-Reyes, R. Fernández-Climent, S. Masi, C. A. Mesa, C. Echeverría-Arrondo, F. Aiello, F. Balzano, G. Uccello-Barretta, J. Rodríguez-Pereira, S. Giménez and I. Mora-Seró, Efficient Ligand Passivation Enables Ultra stable $CsPbX_3$ Perovskite Nanocrystals in Fully Alcohol Environments, *Adv. Opt. Mater.*, 2023, **11**, 2203096.

86 L. Zhang, W. Liang, L. Xu, M. Zhu, X. Wang, J. Su, L. Li, N. Liu, Z. Zhang and Y. Gao, Room-Temperature Quaternary Alkylammonium Passivation toward Morphology-Controllable $CsPbBr_3$ Nanocrystals with Excellent Luminescence and Stability for White LEDs, *Chem. Eng. J.*, 2021, **417**, 129349.

87 J. Xue, R. Wang and Y. Yang, The Surface of Halide Perovskites from Nano to Bulk, *Nat. Rev. Mater.*, 2020, **5**, 809–827.

88 N. F. Maneiro, K. Sun, I. L. Fernández, S. G. Graña, P. M. Buschbaum and L. Polavarapu, Ligand Chemistry of Inorganic Lead Halide Perovskite Nanocrystals, *ACS Energy Lett.*, 2023, **8**, 1152–1191.

89 F. Li, Y. Liu, H. Wang, Q. Zhan, Q. Liu and Z. Xia, Postsynthetic Surface Trap Removal of $CsPbX_3$ (X = Cl, Br, or I) Quantum Dots via a ZnX_2/Hexane Solution toward an Enhanced Luminescence Quantum Yield, *Chem. Mater.*, 2018, **30**, 8546–8554.

90 A. Marronnier, G. Roma, S. Boyer-Richard, L. Pedesseau, J.-M. Jancu, Y. Bonnassieux, C. Katan, C. C. Stoumpos, M. G. Kanatzidis and J. Even, Anharmonicity and Disorder in the Black Phases of Cesium Lead Iodide Used for Stable Inorganic Perovskite Solar Cells, *ACS Nano*, 2018, **12**, 3477–3486.

91 C. Wang, A. S. R. Chesmanb and J. J. Jasieniak, Stabilizing the Cubic Perovskite Phase of $CsPbI_3$ Nanocrystals by Using an Alkyl Phosphinic Acid, *Chem. Commun.*, 2017, **53**, 232–235.

Published on 27 de setembre 2023. Downloaded on 11/2/2026 22:48:11.

92 F. Krieg, S. T. Ochsenbein, S. Yakunin, S. ten Brinck, P. Aellen, A. Suess, B. Clerc, D. Guggisberg, O. Nazarenko, Y. Shynkarenko, S. Kumar, C.-J. Shih, I. Infante and M. V. Kovalenko, Colloidal $CsPbX_3$ (X = Cl, Br, I) Nanocrystals 2.0: Zwitterionic Capping Ligands for Improved Durability and Stability, *ACS Energy Lett.*, 2018, **3**, 641–646.

93 S. H. Noh, W. J. Jeong, K. H. Lee, H. S. Yang, E. H. Suh, J. Jung, S. C. Park, D. Lee, I. H. Jung, Y. J. Jeong and J. Jang, Photocrosslinkable Zwitterionic Ligands for Perovskite Nanocrystals: Self-Assembly and High-Resolution Direct Patterning, *Adv. Funct. Mater.*, 2023, 2304004.

94 H. Zhu, M. Kick, M. Ginterseder, C. J. Krajewska, T. Šverko, R. Li, Y. Lu, M.-C. Shih, T. V. Voorhis and M. G. Bawendi, Synthesis of Zwitterionic $CsPbBr_3$ Nanocrystals with Controlled Anisotropy using Surface-Selective Ligand Pairs, *Adv. Mater.*, 2023, 2304069.

95 S. Guo, H. Liu, H. He, W. Wang, L. Jiang, X. Xiong and L. Wang, Eco-Friendly Strategy to Improve Durability and Stability of Zwitterionic Capping Ligand Colloidal $CsPbBr_3$ Nanocrystals, *Langmuir*, 2020, **36**, 6775–6781.

96 F. Liu, Y. Zhang, C. Ding, S. Kobayashi, T. Izuishi, N. Nakazawa, T. Toyoda, T. Ohta, S. Hayase, T. Minemoto, K. Yoshino, S. Dai and Q. Shen, Highly Luminescent Phase-Stable $CsPbI_3$ Perovskite Quantum Dots Achieving Near 100% Absolute Photoluminescence Quantum Yield, *ACS Nano*, 2017, **11**, 10373–10383.

97 T. Wang, X. Li, T. Fang, S. Wang and J. Song, Room-Temperature Synthesis of Perovskite-Phase $CsPbI_3$ Nanocrystals for Optoelectronics via a Ligand-Mediated Strategy, *Chem. Eng. J.*, 2021, **418**, 129361.

98 L. Wu, Q. Zhong, D. Yang, M. Chen, H. Hu, Q. Pan, H. Liu, M. Cao, Y. Xu and B. Sun, Improving the Stability and Size Tunability of Cesium Lead Halide Perovskite Nanocrystals Using Trioctylphosphine Oxide as the Capping Ligand, *Langmuir*, 2017, **33**, 12689–12696.

99 M. R. Alpert, J. S. Niezgoda, A. Z. Chen, B. J. Foley, S. Cuthriell, L. U. Yoon and J. J. Choi, Colloidal Nanocrystals as A Platform for Rapid Screening of Charge Trap Passivating Molecules for Metal Halide Perovskite Thin Films, *Chem. Mater.*, 2018, **30**, 4515–4526.

100 X. Min, Q. Xie, Z. Wang, X. Wang and M. Chen, Improving the Stability and Optical Properties of $CsPbI_3$ Perovskite Nanocrystals by 1-Octadecanethiol through Surface Modification, *Mater. Chem. Phys.*, 2022, **276**, 125404.

101 J. Zhang, C. Yin, F. Yang, Y. Yao, F. Yuan, H. Chen, R. Wang, S. Bai, G. Tu and L. Hou, Highly Luminescent and Stable $CsPbI_3$ Perovskite Nanocrystals with Sodium Dodecyl Sulfate Ligand Passivation for Red-Light-Emitting Diodes, *J. Phys. Chem. Lett.*, 2021, **12**, 2437–2443.

102 S. Baek, Y. Kim and S. Kim, Highly Photo-Stable $CsPbI_3$ Perovskite Quantum Dots via Thiol Ligand Exchange and Their Polymer Film Application, *J. Ind. Eng. Chem.*, 2020, **83**, 279–284.

103 D. Yang, X. Li, W. Zhou, S. Zhang, C. Meng, Y. Wu, Y. Wang and H. Zeng, $CsPbBr_3$ Quantum Dots 2.0: Benzenesulfonic Acid Equivalent Ligand Awakens Complete Purification, *Adv. Mater.*, 2019, **31**, 1900767.

104 D. Yang, X. Li, Y. Wu, C. Wei, Z. Qin, C. Zhang, Z. Sun, Y. Li, Y. Wang and H. Zeng, Surface Halogen Compensation for Robust Performance Enhancements of $CsPbX_3$ Perovskite Quantum Dots, *Adv. Opt. Mater.*, 2019, **7**, 1900276.

105 F. Stasio, S. Christodoulou, N. Huo and G. Konstantatos, Near-Unity Photoluminescence Quantum Yield in $CsPbBr_3$ Nanocrystal Solid-State Films via Postsynthesis Treatment with Lead Bromide, *Chem. Mater.*, 2017, **29**, 7663–7667.

106 J. Woo, Y. Kim, J. Bae, T. Kim, J. Kim, D. C. Lee and S. Jeong, Highly Stable Cesium Lead Halide Perovskite Nanocrystals through in Situ Lead Halide Inorganic Passivation, *Chem. Mater.*, 2017, **29**, 7088–7092.

107 H. Li, Y. Qian, X. Xing, J. Zhu, X. Huang, Q. Jing, W. Zhang, C. Zhang and Z. Lu, Enhancing Luminescence and Photostability of $CsPbBr_3$ Nanocrystals via Surface Passivation with Silver Complex, *J. Phys. Chem. C*, 2018, **122**, 12994–13000.

108 B. J. Bohn, Y. Tong, M. Gramlich, M. Lai, M. Döblinger, K. Wang, R. L. Z. Hoye, P. Müller-Buschbaum, S. D. Stranks, A. S. Urban, L. Polavarapu and J. Feldmann, Boosting Tunable Blue Luminescence of Halide Perovskite Nanoplatelets through Postsynthetic Surface Trap Repair, *Nano Lett.*, 2018, **18**, 5231–5238.

109 G. H. Ahmed, J. K. Demellawi, J. Yin, J. Pan, D. Velusamy, M. Hedhili, E. Alarousu, O. M. Bakr, H. N. Alshareef and O. F. Mohammed, Giant Photoluminescence Enhancement in $CsPbCl_3$ Perovskite Nanocrystals by Simultaneous Dual-Surface Passivation, *ACS Energy Lett.*, 2018, **3**, 2301–2307.

110 Y. Xu, Q. Wang, L. Zhang, M. Lyu, H. Lu, T. Bai, F. Liu, M. Wang and J. Zhu, Strontium-Doped $CsPbI_3$ Quantum Dots as an Interfacial Layer for Efficient Inorganic Perovskite Solar Cells, *Sol. RRL*, 2021, **5**, 2100669.

111 C. Bi, X. Sun, X. Huang, S. Wang, J. Yuan, J. Wang, T. Pullerits and J. Tian, Stable $CsPb_{1-x}Zn_xI_3$ Colloidal Quantum Dots with Ultralow Density of Trap States for High-Performance Solar Cells, *Chem. Mater.*, 2020, **32**, 6105–6113.

112 B. A. Koscher, J. K. Swabeck, N. D. Bronstein and A. P. Alivisatos, Trap-Free $CsPbBr_3$ Colloidal Nanocrystals by Postsynthetic Thiocyanate Surface Treatment, *J. Am. Chem. Soc.*, 2017, **139**, 6566–6569.

113 T. Ahmed, S. Seth and A. Samanta, Boosting the Photoluminescence of $CsPbX_3$ (X = Cl, Br, I) Perovskite Nanocrystals Covering a Wide Wavelength Range by Postsynthetic Treatment with Tetrafluoroborate Salts, *Chem. Mater.*, 2018, **30**, 3633–3637.

114 M. Imran, V. Caligiuri, M. Wang, L. Goldoni, M. Prato, R. Krahne, L. De Trizio and L. Manna, Benzoyl Halides as Alternative Precursors for the Colloidal Synthesis of Lead-Based Halide Perovskite Nanocrystals, *J. Am. Chem. Soc.*, 2018, **140**, 2656–2664.

115 P. Liu, W. Chen, W. Wang, B. Xu, D. Wu, J. Hao, W. Cao, F. Fang, Y. Li, Y. Zeng, R. Pan, S. Chen, W. Cao, X. Sun and

 This journal is © The Royal Society of Chemistry and the Chinese Chemical Society 2024

Published on 27 de setembre 2023. Downloaded on 11/2/2026 22:48:11.

K. Wang, Halide-Rich Synthesized Cesium Lead Bromide Perovskite Nanocrystals for Light-Emitting Diodes with Improved Performance, *Chem. Mater.*, 2017, **29**, 5168–5173.

116 W. Song, D. Wang, J. Tian, G. Qi, M. Wu, S. Liu, T. Wang, B. Wang, Y. Yao, Z. Zou and B. Liu, Encapsulation of Dual-Passivated Perovskite Quantum Dots for Bio-Imaging, *Small*, 2022, **18**, 2204763.

117 J. Yao, J. Ge, K. Wang, G. Zhang, B. Zhu, C. Chen, Q. Zhang, Y. Luo, S. Yu and H. Yao, Few-Nanometer-Sized α-$CsPbI_3$ Quantum Dots Enabled by Strontium Substitution and Iodide Passivation for Efficient Red-Light Emitting Diodes, *J. Am. Chem. Soc.*, 2019, **141**, 2069–2079.

118 A. Dutta, S. K. Dutta, S. D. Adhikari and N. Pradhan, Phase-Stable CsPbI3 Nanocrystals: The Reaction Temperature Matters, *Angew. Chem., Int. Ed.*, 2018, **57**, 9083–9087.

119 A. Dutta, R. K. Behera, P. Pal, S. Baitalik and N. Pradhan, Near-Unity Photoluminescence Quantum Efficiency for All $CsPbX_3$ (X = Cl, Br, and I) Perovskite Nanocrystals: A Generic Synthesis Approach, *Angew. Chem.*, 2019, **131**, 5608–5612.

120 Y. Cai, H. Wang, Y. Li, L. Wang, Y. Lv, X. Yang and R. Xie, Trimethylsilyl Iodine-Mediated Synthesis of Highly Bright Red-Emitting $CsPbI_3$ Perovskite Quantum Dots with Significantly Improved Stability, *Chem. Mater.*, 2019, **31**, 881–889.

121 E. Yassitepe, Z. Yang, O. Voznyy, Y. Kim, G. Walters, J. Castañeda, P. Kanjanaboos, M. Yuan, X. Gong, F. Fan, J. Pan, S. Hoogland, R. Comin, O. M. Bakr, L. A. Padilha, A. F. Nogueira and E. H. Sargent, Amine-Free Synthesis of Cesium Lead Halide Perovskite Quantum Dots for Efficient Light-Emitting Diodes, *Adv. Funct. Mater.*, 2016, **26**, 8757–8763.

122 A. Loiudice, S. Saris, E. Oveisi, D. T. L. Alexander and R. Buonsanti, CsPbBr3 QD/AlOx Inorganic Nanocomposites with Exceptional Stability in Water, Light, and Heat, *Angew. Chem., Int. Ed.*, 2017, **56**, 10696–10701.

123 H. C. Wang, S. Y. Lin, A. C. Tang, B. P. Singh, H. C. Tong, C. Y. Chen, Y. C. Lee, T. L. Tsai and R. S. Liu, Mesoporous Silica Particles Integrated with All-Inorganic $CsPbBr_3$ Perovskite Quantum-Dot Nanocomposites (MP-PQDs) with High Stability and Wide Color Gamut Used for Backlight Display, *Angew. Chem., Int. Ed.*, 2016, **55**, 7924–7929.

124 C. Sun, Y. Zhang, C. Ruan, C. Yin, X. Wang, Y. Wang and W. W. Yu, Efficient and Stable White LEDs with Silica-Coated Inorganic Perovskite Quantum Dots, *Adv. Mater.*, 2016, **28**, 10088–10094.

125 X. Li, Y. Wang, H. Sun and H. Zeng, Amino-Mediated Anchoring Perovskite Quantum Dots for Stable and Low-Threshold Random Lasing, *Adv. Mater.*, 2017, **29**, 1701185.

126 C. Rossi, R. Scarfiello, R. Brescia, L. Goldoni, G. Caputo, L. Carbone, D. Colombara, L. Trizio, L. Manna and D. Baranov, Exploiting the Transformative Features of Metal Halides for the Synthesis of CsPbBr3@SiO_2 Core–Shell Nanocrystals, *Chem. Mater.*, 2022, **34**, 405–413.

127 E. M. Sanehira, A. R. Marshall, J. A. Christians, S. P. Harvey, P. N. Ciesielski, L. M. Wheeler, P. Schulz, L. Y. Lin, M. C. Beard and J. M. Luther, Enhanced Mobility CsPbI3 Quantum Dot Arrays for Record-Efficiency, High-Voltage Photovoltaic cells, *Sci. Adv.*, 2017, **3**, eaao4204.

128 D. Yang, X. Li, W. Zhou, S. Zhang, C. Meng, Y. Wu, Y. Wang and H. Zeng, $CsPbBr_3$ Quantum Dots 2.0: Benzenesulfonic Acid Equivalent Ligand Awakens Complete Purification, *Adv. Mater.*, 2019, **31**, 1900767.

129 E. J. D. Klem, D. D. MacNeil, P. W. Cyr, L. Levina and E. H. Sargenta, Efficient Solution-Processed Infrared Photovoltaic Cells: Planarized All-Inorganic Bulk Heterojunction Devices via Inter-Quantum-Dot Bridging During Growth from Solution, *Appl. Phys. Lett.*, 2007, **90**, 183113.

130 L. M. Wheeler, E. M. Sanehira, A. R. Marshall, P. Schulz, M. Suri, N. C. Anderson, J. A. Christians, D. Nordlund, D. Sokaras, T. Kroll, S. P. Harvey, J. J. Berry, L. Y. Lin and J. M. Luther, Targeted Ligand-Exchange Chemistry on Cesium Lead Halide Perovskite Quantum Dots for High-Efficiency Photovoltaics, *J. Am. Chem. Soc.*, 2018, **140**, 10504–10513.

131 S. Song, Y. Lyu, B. Cao and W. Wang, Surface Modification Strategy Synthesized $CsPbX_3$ Perovskite Quantum Dots with Excellent Stability and Optical Properties in Water, *Adv. Funct. Mater.*, 2023, **33**, 2300493.

132 Z. Li, L. Kong, S. Huang and L. Li, Highly Luminescent and Ultrastable $CsPbBr_3$ Perovskite Quantum Dots Incorporated into a Silica/Alumina Monolith, *Angew. Chem.*, 2017, **129**, 8246–8250.

133 J. Sun, S. Huang, X. Liu, Q. Xu, Q. Zhang, W. Jiang, D. Xue, J. Xu, J. Ma, J. Ding, Q. Ge, L. Gu, X. Fang, H. Zhong, J. Hu and L. Wan, Polar Solvent Induced Lattice Distortion of Cubic $CsPbI_3$ Nanocubes and Hierarchical Self-Assembly into Orthorhombic Single-Crystalline Nanowires, *J. Am. Chem. Soc.*, 2018, **140**, 11705–11715.

134 C. Wei, W. Su, J. Li, B. Xu, Q. Shan, Y. Wu, F. Zhang, M. Luo, H. Xiang, Z. Cui and H. Zeng, A Universal Ternary-Solvent-Ink Strategy toward Efficient Inkjet-Printed Perovskite Quantum Dot Light-Emitting Diodes, *Adv. Mater.*, 2022, **34**, 2107798.

135 Y. Xu, P. Niu, L. Zhang, Z. Wen, S. Cheng, M. Lyu and J. Zhu, Tailoring Multifunctional Anions to Inhibit Methanol Absorption on a $CsPbBr_3$ Quantum Dot Surface for Highly Efficient Semi-Transparent Photovoltaics, *Nanoscale*, 2023, **15**, 9691–9699.

136 J. Kim, B. Koo, W. H. Kim, J. Choi, C. Choi, S. J. Lim, J.-S. Lee, D.-H. Kim, M. J. Ko and Y. Kim, Alkali Acetate-Assisted Enhanced Electronic Coupling in $CsPbI_3$ Perovskite Quantum Dot Solids for Improved Photovoltaics, *Nano Energy*, 2019, **66**, 104130.

137 J. Kim, S. Cho, F. Dinic, J. Choi, C. Choi, S. M. Jeong, J. Lee, O. Voznyy, M. J. Ko and Y. Kim, Hydrophobic Stabilizer-Anchored Fully Inorganic Perovskite Quantum Dots Enhance Moisture Resistance and Photovoltaic Performance, *Nano Energy*, 2020, **75**, 104985.

138 D. Jia, J. Chen, J. Qiu, H. Ma, M. Yu, J. Liu and X. Zhang, Tailoring Solvent-Mediated Ligand Exchange for $CsPbI_3$ Perovskite Quantum Dot Solar Cells with Efficiency Exceeding 16.5%, *Joule*, 2022, **6**, 1–8.

Published on 27 de setembre 2023. Downloaded on 11/2/2026 22:48:11.

139 A. Hazarika, Q. Zhao, E. A. Gaulding, J. A. Christians, B. Dou, A. R. Marshall, T. Moot, J. J. Berry, J. C. Johnson and J. M. Luther, Perovskite Quantum Dot Photovoltaic Materials beyond the Reach of Thin Films: Full-Range Tuning of A-Site Cation Composition, *ACS Nano*, 2018, **12**, 10327–10337.

140 D. Jia, J. Chen, R. Zhuang, Y. Hua and X. Zhang, Antisolvent-Assisted in Situ Cation Exchange of Perovskite Quantum Dots for Efficient Solar Cells, *Adv. Mater.*, 2023, **35**, 2212160.

141 D. Jia, J. Chen, M. Yu, J. Liu, E. M. J. Johansson, A. Hagfeldt and X. Zhang, Dual Passivation of $CsPbI_3$ Perovskite Nanocrystals with Amino Acid Ligands for Efficient Quantum Dot Solar Cells, *Small*, 2020, **16**, 2001772.

142 Y. Wang, J. Yuan, X. Zhang, X. Ling, B. W. Larson, Q. Zhao, Y. Yang, Y. Shi, J. M. Luther and W. Ma, Surface Ligand Management Aided by a Secondary Amine Enables Increased Synthesis Yield of $CsPbI_3$ Perovskite Quantum Dots and High Photovoltaic Performance, *Adv. Mater.*, 2020, **32**, 2000449.

143 X. Ling, S. Zhou, J. Yuan, J. Shi, Y. Qian, B. W. Larson, Q. Zhao, C. Qin, F. Li, G. Shi, C. Stewart, J. Hu, X. Zhang, J. M. Luther, S. Duhm and W. Ma, 14.1% $CsPbI_3$ Perovskite Quantum Dot Solar Cells via Cesium Cation Passivation, *Adv. Energy Mater.*, 2019, **9**, 1900721.

144 H. Meng, Z. Shao, L. Wang, Z. Li, R. Liu, Y. Fan, G. Cui and S. Pang, Chemical Composition and Phase Evolution in DMAI-Derived Inorganic Perovskite Solar Cells, *ACS Energy Lett.*, 2020, **5**, 263–270.

145 S. Yoon, H. Min, J. B. Kim, G. Kim, K. S. Lee and S. Seok, Surface Engineering of Ambient-Air-Processed Cesium Lead Triiodide Layers for Efficient Solar Cells, *Joule*, 2021, **5**, 183–196.

146 S. Fu, J. Le, X. Guo, N. Sun, W. Zhang, W. Song and J. Fang, Polishing the Lead-Poor Surface for Efficient Inverted $CsPbI_3$ Perovskite Solar Cells, *Adv. Mater.*, 2022, **34**, 2205066.

147 Y. Wang, M. I. Dar, L. K. Ono, T. Zhang, M. Kan, Y. Li, L. Zhang, X. Wang, Y. Yang, X. Gao, Y. Qi, M. Grätzel and Y. Zhao, Thermodynamically Stabilized β-$CsPbI_3$-Based Perovskite Solar Cells with Efficiencies >18%, *Science*, 2019, **365**, 591–595.

148 X. Sun, Z. Shao, Z. Li, D. Liu, C. Gao, C. Chen, B. Zhang, L. Hao, Q. Zhao, Y. Li, X. Wang, Y. Lu, X. Wang, G. Cui and S. Pang, Highly Efficient $CsPbI_3/Cs_{1-x}DMA_xPbI_3$ Bulk Heterojunction Perovskite Solar Cell, *Joule*, 2022, **6**, 850–860.

149 C. Xu, S. Zhang, W. Fan, F. Cheng, H. Sun, Z. Kang and Y. Zhang, Pushing the Limit of Open-Circuit Voltage Deficit via Modifying Buried Interface in $CsPbI_3$ Perovskite Solar Cells, *Adv. Mater.*, 2023, **35**, 2207172.

150 S. Tan, C. Tan, Y. Cui, B. Yu, Y. Li, H. Wu, J. Shi, Y. Luo, D. Li and Q. Meng, Constructing an Interfacial Gradient Heterostructure Enables Efficient $CsPbI_3$ Perovskite Solar Cells and Printed Minimodules, *Adv. Mater.*, 2023, **35**, 2301879.

151 X. Ling, J. Yuan, X. Zhang, Y. Qian, S. M. Zakeeruddin, B. W. Larson, Q. Zhao, J. Shi, J. Yang, K. Ji, Y. Zhang, Y. Wang, C. Zhang, S. Duhm, J. M. Luther, M. Grätzel and W. Ma, Guanidinium-Assisted Surface Matrix Engineering for Highly Efficient Perovskite Quantum Dot Photovoltaics, *Adv. Mater.*, 2020, **32**, 2001906.

152 R. Wang, J. Xue, K. Wang, Z. Wang, Y. Luo, D. Fenning, G. Xu, S. Nuryyeva, T. Huang, Y. Zhao, J. Yang, J. Zhu, M. Wang, S. Tan, I. Yavuz, K. N. Houk and Y. Yang, Constructive Molecular Configurations for Surface-Defect Passivation of Perovskite Photovoltaics, *Science*, 2019, **366**, 1509–1513.

153 H. Zhou, L. Yang, Y. Duan, M. Wu, Y. Li, D. Xu, H. Zou, J. Wang, S. Yang and Z. Liu, 24.96%-Efficiency $FACsPbI_3$ Perovskite Solar Cells Enabled by an Asymmetric 1,3-Thiazole-2,4-Diammonium, *Adv. Energy Mater.*, 2023, **13**, 2204372.

154 P. Qin, G. Yang, Z. Ren, S. H. Cheung, S. K. So, L. Chen, J. Hao, J. Hou and G. Li, Stable and Efficient Organo-Metal Halide Hybrid Perovskite Solar Cells via π-Conjugated Lewis Base Polymer Induced Trap Passivation and Charge Extraction, *Adv. Mater.*, 2018, **30**, 1706126.

155 X. Yue, X. Zhao, B. Fan, Y. Yang, L. Yan, S. Qu, H. Huang, Q. Zhang, H. Yan, P. Cui, J. Ji, J. Ma and M. Li, Surface Regulation through Dipolar Molecule Boosting the Efficiency of Mixed 2D/3D Perovskite Solar Cell to 24%, *Adv. Funct. Mater.*, 2023, **33**, 2209921.

156 S. You, H. Wang, S. Bi, J. Zhou, L. Qin, X. Qiu, Z. Zhao, Y. Xu, Y. Zhang, X. Shi, H. Zhou and Z. Tang, A Biopolymer Heparin Sodium Interlayer Anchoring TiO_2 and $MAPbI_3$ Enhances Trap Passivation and Device Stability in Perovskite Solar Cells, *Adv. Mater.*, 2018, **30**, 1706924.

157 J. Khan, X. Zhang, J. Yuan, Y. Wang, G. Shi, R. Patterson, J. Shi, X. Ling, L. Hu, T. Wu, S. Dai and W. Ma, Tuning the Surface-Passivating Ligand Anchoring Position Enables Phase Robustness in $CsPbI_3$ Perovskite Quantum Dot Solar Cells, *ACS Energy Lett.*, 2020, **5**, 3322–3329.

158 J. Chen, D. Jia, J. Qiu, R. Zhuang, Y. Hua and X. Zhang, Multidentate Passivation Crosslinking Perovskite Quantum Dots for Efficient Solar Cells, *Nano Energy*, 2022, **96**, 107140.

159 Q. Zhou, J. Duan, J. Du, Q. Guo, Q. Zhang, X. Yang, Y. Duan and Q. Tang, Tailored Lattice "Tape" to Confine Tensile Interface for 11.08%-Efficiency All-Inorganic $CsPbBr_3$ Perovskite Solar Cell with an Ultrahigh Voltage of 1.702 V, *Adv. Sci.*, 2021, **8**, 2101418.

160 J. Wang, P. Zhao, Y. Hu, Z. Lin, J. Su, J. Zhang, J. Chang and Y. Hao, An Exploration of All-Inorganic Perovskite/Gallium Arsenide Tandem Solar Cells, *Sol. RRL*, 2021, **5**, 2100121.

161 F. Hou, Y. Li, L. Yan, B. Shi, N. Ren, P. Wang, D. Zhang, H. Ren, Y. Ding, Q. Huang, T. Li, Y. Li, Y. Zhao and X. Zhang, Control Perovskite Crystals Vertical Growth for Obtaining High-Performance Monolithic Perovskite/Silicon Heterojunction Tandem Solar Cells with V_{OC} of 1.93 V, *Sol. RRL*, 2021, **5**, 2100357.

162 C. Yang, C. Zhao, Y. Sun, Q. Li, M. R. Islam, K. Liu, Z. Wang, S. N. Qu and Z. Wang, Optical Management in Organic Photovoltaic Devices, *Carbon Energy*, 2021, **3**, 4–23.

Published on 27 de setembre 2023. Downloaded on 11/2/2026 22:48:11.

163 Q. A. Akkerman, M. Gandini, F. D. Stasio, P. Rastogi, F. Palazon1, G. Bertoni, J. M. Ball, M. Prato, A. Petrozza and L. Manna, Strongly Emissive Perovskite Nanocrystal Inks for High-Voltage Solar Cells, *Nat. Energy*, 2016, **2**, 16194.

164 S. Cho, J. Kim, S. M. Jeong, M. J. Ko, J.-S. Lee and Y. Kim, High-Voltage and Green-Emitting Perovskite Quantum Dot Solar Cells via Solvent Miscibility-Induced Solid-State Ligand Exchange, *Chem. Mater.*, 2020, **32**, 8808–8818.

165 X. Zhang, Y. Qian, X. Ling, Y. Wang, Y. Zhang, J. Shi, Y. Shi, J. Yuan and W. Ma, α-$CsPbBr_3$ Perovskite Quantum Dots for Application in Semitransparent Photovoltaics, *ACS Appl. Mater. Interfaces*, 2020, **12**, 27307–27315.

166 Q. Wang, Y. Xu, L. Zhang, P. Niu, R. Zhou, M. Lyu, H. Lu and J. Zhu, Aromatic Carboxylic Acid Ligand Management for $CsPbBr_3$ Quantum Dot Light-Emitting Solar Cells, *ACS Appl. Nano Mater.*, 2022, **5**, 10495–10503.

167 J. A. Dias, S. H. Santagneli, S. J. L. Ribeiro and Y. Messaddeq, An Overview of the Current Advances and Future Perspectives, *Sol. RRL*, 2021, **5**, 2100205.

168 Z. Yang, A. Janmohamed, X. Lan, F. Pelayo García de Arquer, O. Voznyy, E. Yassitepe, G. Kim, Z. Ning, X. Gong, R. Comin and E. H. Sargent, Colloidal Quantum Dot Photovoltaics Enhanced by Perovskite Shelling, *Nano Lett.*, 2015, **15**, 7539–7543.

169 K. Chen, Q. Zhong, W. Chen, B. Sang, Y. Wang, T. Yang, Y. Liu, Y. Zhang and H. Zhang, Short-Chain Ligand-Passivated Stable α-$CsPbI_3$ Quantum Dot for All-Inorganic Perovskite Solar Cells, *Adv. Funct. Mater.*, 2019, **29**, 1900991.

170 J. Shi, F. Li,L, Y. Jin, C. Liu, B. C.-Kleinstein, S. Yuan, Y. Li, Z. Wang, J. Yuan and W. Ma, In Situ Ligand Bonding Management of CsPbI3 Perovskite Quantum Dots Enables High-Performance Photovoltaics and Red Light-Emitting Diodes, *Angew. Chem., Int. Ed.*, 2020, **59**, 22230–22237.

171 X. Zhang, H. Huang, Y. Maung, J. Yuan and W. Ma, Aromatic Amine-Assisted Pseudo-Solution-Phase Ligand Exchange in $CsPbI_3$ Perovskite Quantum Dot Solar Cells, *Chem. Commun.*, 2021, **57**, 7906–7909.

172 D. Jia, J. Chen, R. Zhuang, Y. Hua and X. Zhang, Inhibiting Lattice Distortion of $CsPbI_3$ Perovskite Quantum Dots for Solar Cells with Efficiency Over 16.6%, *Energy Environ. Sci.*, 2022, **15**, 4201–4212.

173 C. Liu, Q. Zeng, Y. Zhao, Y. Yu, M. Yang, H. Gao, H. Wei and B. Yang, Surface Ligands Management for Efficient $CsPbBrI_2$ Perovskite Nanocrystal Solar Cells, *Sol. RRL*, 2020, **4**, 2000102.

174 M. M. Byranvand, C. O.-Martínez, J. Ye, W. Zuo, L. Manna, M. Saliba, R. L. Z. Hoye and L. Polavarapu, Recent Progress in Mixed A-Site Cation Halide Perovskite Thin-Films and Nanocrystals for Solar Cells and Light-Emitting Diodes, *Adv. Opt. Mater.*, 2022, **10**, 2200423.

175 A. Hazarika, Q. Zhao, E. A. Gaulding, J. A. Christians, B. Dou, A. R. Marshall, T. Moot, J. J. Berry, J. C. Johnson and J. M. Luther, Perovskite Quantum Dot Photovoltaic Materials beyond the Reach of Thin Films: Full-Range Tuning of A-Site Cation Composition, *ACS Nano*, 2018, **12**, 10327–10337.

176 M. Hao, Y. Bai, S. Zeiske, L. Ren, J. Liu, Y. Yuan, N. Zarrabi, N. Cheng, M. Ghasemi, P. Chen, M. Lyu, D. He, J. Yun, Y. Du, Y. Wang, S. Ding, A. Armin, P. Meredith, G. Liu, H. Cheng and L. Wang, Ligand-assisted Cation-Exchange Engineering for High-Efficiency Colloidal $Cs_{1-x}FA_xPbI_3$ Quantum Dot Solar Cells with Reduced Phase Segregation, *Nat. Energy*, 2020, **5**, 79–88.

177 D. Jia, J. Chen, R. Zhuang, Y. Hua and X. Zhang, Antisolvent-Assisted in Situ Cation Exchange of Perovskite Quantum Dots for Efficient Solar Cells, *Adv. Mater.*, 2023, **35**, 2212160.

178 L. Zhang, C. Kang, G. Zhang, Z. Pan, Z. Huang, S. Xu, H. Rao, H. Liu, S. Wu, X. Wu, X. Li, Z. Zhu, X. Zhong and A. K.-Y. Jen, All-Inorganic $CsPbI_3$ Quantum Dot Solar Cells with Efficiency over 16% by Defect Control, *Adv. Funct. Mater.*, 2020, **31**, 2005930.

179 J. Shi, B. Kleinstein, X. Zhang, C. Zhao, Y. Zhang, X. Ling, J. Guo, D.-H. Ko, B. Xu, J. Yuan and W. Ma, In Situ Iodide Passivation Toward Efficient CsPbI3 Perovskite Quantum Dot Solar Cells, *Nano-Micro Lett.*, 2023, **15**, 163.

180 Y. Qian, Y. Shi, G. Shi, G. Shi, X. Zhang, L. Yuan, Q. Zhong, Y. Liu, Y. Wang, X. Ling, F. Li, M. Cao, S. Li, Q. Zhang, Z. Liu and W. Ma, The Impact of Precursor Ratio on the Synthetic Production, Surface Chemistry, and Photovoltaic Performance of CsPbI3 Perovskite Quantum Dots, *Sol. RRL*, 2021, **5**, 2100090.

181 J. Chen, D. Jia, R. Zhuang, Y. Hua and X. Zhang, Highly Orientated Perovskite Quantum Dot Solids for Efficient Solar Cells, *Adv. Mater.*, 2022, **34**, 2204259.

182 D. Jia, J. Chen, X. Mei, W. Fan, S. Luo, M. Yu, J. Liu and X. Zhang, Surface Matrix Curing of Inorganic $CsPbI_3$ Perovskite Quantum Dots for Solar Cells with Efficiency Over 16%, *Energy Environ. Sci.*, 2021, **14**, 4599–4609.